PLANAR 4R LINKAGE KINEMATIC SYNTHESIS AND ANALYSIS TUTORIAL

M. John D. Hayes, Mirja Rotzoll, Alia Nichol, Atena Ourdas, Quinn A. Bucciol
Department of Mechanical and Aerospace Engineering, Carleton University, Ottawa, ON K1S 5B6, Canada
Email: john.hayes@carleton.ca; mirjarotzoll@cmail.carleton.ca; alianichol@cmail.carleton.ca; atenaourdas@gmail.com; quinnabucciol@gmail.com

ABSTRACT

A complete classification scheme of the relative mobility characteristics of each link for every planar 4R[1] linkage reported in this paper is obtained in a novel and efficient way. To lay the foundation of this work, recent results are first briefly summarised. The algebraic input-output (IO) equation for any planar 4R linkage is obtained. The coefficients factor into four pairs of bilinear terms in the design parameters, the directed lengths of the four links. These eight bilinear factors can be viewed as the eight plane faces of a regular stellated octahedron in the three-dimensional projective space implied by the four design parameter directed lengths which may be interpreted as the four homogeneous coordinates of the space. The location of a point in this parameter space relative to the octahedron predicts the mobility of the linkage. The numerical values of the eight bilinear factors of the algebraic IO equation imply a complete classification scheme for the relative mobility characteristics of the four links of these planar four-bar mechanisms.

This version of the paper is more comprehensive than the conference version, and intended for use as a reference for the Project in MAAE 3004, Dynamics of Machinery. This version of the paper also includes detailed notes on: exact kinematic synthesis of planar function generators using the algebraic IO equation; the three species of double points of algebraic curves and their implications for the relative mobility of the 4R links; the projective extension of the Euclidean plane of the mechanism motion; interpretation of the IO curves of mechanisms; angular velocity and acceleration level IO equation, and finally; determining 4R mechanism coupler point curves. All other information, kinematics and kinetics, required to successfully complete the tasks demanded by the project will be presented in the course lectures and may also be found in the MAAE 3004 recommended textbook: *Theory of Machines and Mechanisms, 6$^{\text{th}}$ edition* by Uicker, Pennock, and Shigley.

Keywords: planar 4R linkages; kinematic synthesis; double points of planar algebraic equations; design parameter space; link relative mobility classification; coupler point curves.

[1] This terminology refers to a mechanical system comprising four rigid links connected to each other with four sequential revolute joints (R-pairs) forming a closed 4R kinematic chain.

1. INTRODUCTION

As James T. Kirk, Captain of the Starship Enterprise, may one day say many thousands of years from now in a galaxy far, far away: "In the firmament of mechanical design the four-bar linkage burns as it's brightest star [1]." Indeed, four-bar linkages are ubiquitous. They can be identified in mechanical systems we encounter every day: mechanical pencils; fold-out table-tops in class room chairs; bicycle lock mechanisms; etc.. Ever since humans had the ability to formulate abstract thoughts, for countless thousands of years, four-bar linkages, in their many forms, have been used to perform a large variety of tasks everywhere there have been human beings [2]. However, only in the last 3000 years have the engineering sciences been applied, in ever increasingly more sophisticated ways, to the synthesis and analysis of linkages for achieving desired outputs for given inputs [3]. The science of mechanisms has evolved such that now nearly every article of clothing you wear, the vehicles you are transported by, the household devices you use, even the streets you walk on have all been touched by at least one, or two, if not many thousands, of four-bar linkages. These mechanical systems can be designed to generate general displacements and motions in 3D space, on the surface of a sphere, and in 2D space which we will call the Euclidean plane.

The term *kinematic pair* indicates a joint between *two* links, hence the use of the word *pair*. Joints are mechanical constraints imposed on the links. Those involving surface contact are called *lower pairs*. Those normally involving point, line, or curve contact are *higher pairs*. Lower pairs enjoy innate practical advantages over higher pairs: applied loads are spread continuously over the contacting surfaces; they can, in general, be more easily and accurately manufactured. There are six types of lower pair (see Figure 1) classified in the following way [4].

1. **R-Pair.** The revolute R-pair is made up of two congruent mating surfaces of revolution. It has one rotational degree-of-freedom (DOF) about its axis.

2. **P-Pair.** The prismatic P-pair comprises two congruent non-circular cylinders, or prisms. It has one translational DOF. It's axis is a line at infinity orthogonal to the direction of translation.

3. **H-Pair.** The helical H-pair, or screw, consists of two congruent helicoidal surfaces whose elements are a convex screw and a concave nut. For an angle θ of relative rotation about the screw axis there is a coupled translation of distance S in a direction parallel to the screw axis. The sense of translation depends on the *hand* of the screw threads and on the sense of rotation. The distance S is the thread *pitch* for a rotation of $\theta = 360^\circ$. When $S = 0$ it becomes an R-pair; when $S = \infty$ it becomes a P-pair. The H-pair has one DOF specified as a translation or a rotation, coupled by the pitch S.

4. **C-Pair.** The cylindrical C-pair consists of mating convex and concave circular cylinders. They can rotate relative to each other about their common axis, and translate relative to each other in a direction parallel to the axis. Hence the C-pair has two DOF: one rotational, the other translational.

5. **S-Pair.** The spherical S-pair, also called *ball-joints*, consists of a solid sphere which exactly conforms with a spherical shell. S-pairs permit three rotational DOF about intersecting orthogonal axes.

6. **E-Pair.** The planar E-pair (for the German word "ebene", meaning "plane") is a special S-pair comprising two concentric spheres of infinite radius. They permit two orthogonal translations and one rotational DOF about an axis orthogonal to the plane of translation. They provide three DOF in total.

In one class of applications, the four-bar mechanism is driven by a human actuator. Examples of this class are numerous, and sometimes taken for granted, e.g., when cutting a paper sheet with scissors, when pedalling a bicycle, etc.. In the case of scissors, the two blades of this tool form a two-link open chain coupled by an R-pair. When held by a user, this chain is coupled to a second, similar chain formed by the

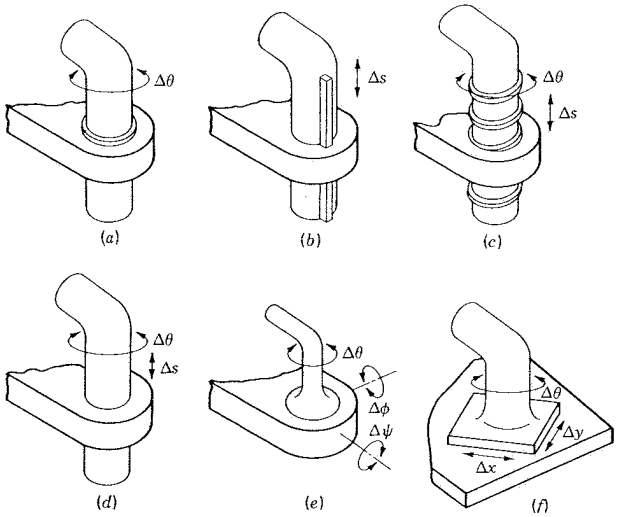

Fig. 1. The six lower pairs: (a) revolute or pin; (b) prismatic; (c) helical; (d) cylindrical; (e) spherical; (f) planar.

Table 1. Summary of the lower pairs and their respective DOF.

Pair type	Symbol	DOF
Revolute	R	1
Prismatic	P	1
Helical	H	1
Cylindrical	C	2
Spherical	S	3
Planar	E	3

proximal phalanx of the thumb and the intermediate phalanx of the index finger, thereby forming a four-bar linkage. Likewise, in the case of a bicycle, the frame and one of the two pedals form an open chain, which couples with a second, similar chain, formed by the calf and the thigh of a human user, coupled by the R-pair of the knee, thereby forming, again, a four-bar linkage.

In the context of planar mechanism kinematics, a *dyad* is a single rigid body link coupled to two other rigid bodies with two kinematic pairs. The two other rigid bodies are a relatively non-moving ground link, while the other is the coupler, which is connected to another dyad thereby forming a closed-loop four-bar mechanism. The coupler is the link that joins, or couples, the two dyads. For planar displacements there are only two types of lower pair that can be used to generate a motion in the plane: R- and P-pairs. This means there are only four practical planar dyads

RR, PR, RP, and PP.

These 3-link serially connected open kinematic chains of rigid bodies are the building blocks of every planar mechanism. They are designated according to the type of joints connecting the rigid links, and listed in series starting with the joint connected to ground, each illustrated in Figure 2.

When a pair of dyads are coupled to each other, a four-bar linkage is obtained. However, the designation

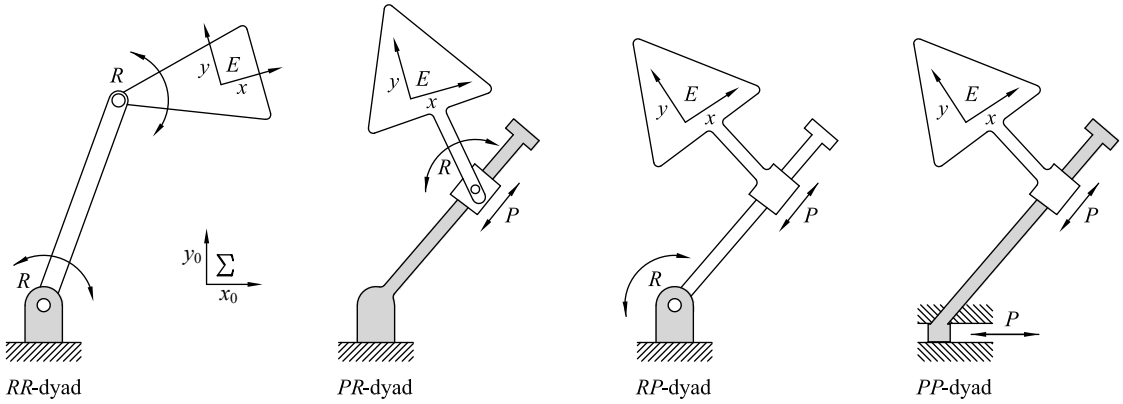

Fig. 2. Types of dyads.

of the *output* dyad may change. For example, consider a planar four-bar linkage composed of an *RR*-dyad on the *left-hand side* of the mechanism, and a PR-dyad on the *right-hand side*, where the *input* link is the *grounded* link in the RR-dyad and the *output* link is the slider of the PR-dyad, see Figure 3.

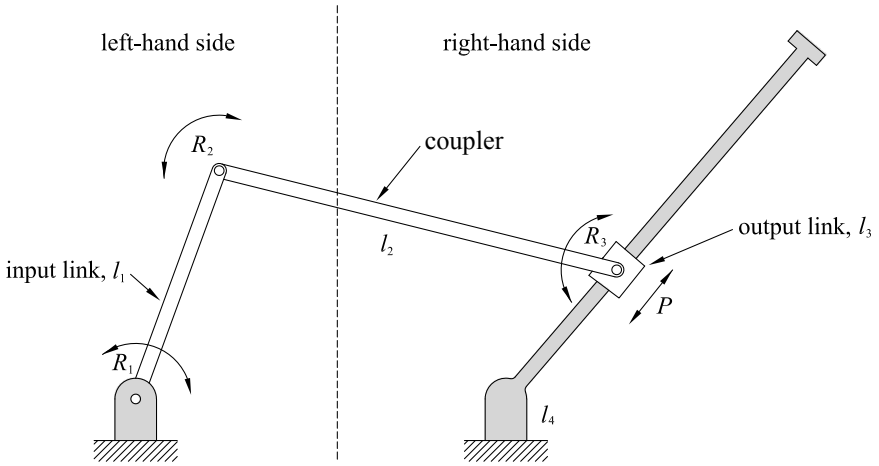

Fig. 3. A four-bar linkage with RR-dyad on the left-hand side and PR-dyad on the right-hand side coupled via link l_2 creates an RRRP mechanism.

Suppose revolute joint R_1 is actuated by some form of torque supplied by an electric rotary motor transferred by a transmission, in turn driving the input link, l_1. The linkage is designated by listing the joints in sequence from the ground fixed actuated joint, starting with the input link listing the joints in order. Thus, the mechanism composed of a driving RR-dyad, and an output PR-dyad is called an RRRP linkage, where the order of PR is switched to RP. If the output were an RP-dyad, the mechanism would be an RRPR linkage. If the input were an RP-dyad while the output was an RR-dyad, the resulting mechanism would be an RPRR linkage, with no noticeable alteration in the designation.

Because a four-bar mechanism possesses only a single DOF then only a single actuated input joint will cause the three movable links to move. Two of the links are connected to the fixed base link of the mechanism by either R- or P-pairs. Let us suppose that one of the joints connected to the fixed non-moving link is the actuated joint. Now the other ground fixed link can be caused to move by a change in input of the actuated joint, and the middle link couples the motion of the actuated input link to the non-actuated base fixed

moving link. Hence, the three relatively moving links in a four-bar mechanism are called the input, coupler, and output links respectively. If the mechanism links are joined by two R-pairs and two P-pairs then the coupler can move with general plane motion. That is, a coordinate system painted onto the coupler can both translate and rotate. If the linkage contains more than two P-pairs then the coupler coordinate system can only have curvilinear or linear displacements. For this reason, we will not discuss four-bar mechanisms containing more than two P-pairs.

2. INPUTS REQUIRED TO GENERATE DESIRED OUTPUTS

We will presently briefly discuss the standard output motion generation problems associated with planar, spherical, and spatial four-bar mechanisms. While the input-output (IO) design problems listed next can be applied to mechanical systems of any kind, our focus will be mostly on planar 4R and RRRP mechanisms. The three most common design problems are termed *function generation*, *motion generation*, and *path generation*, which will now be discussed in that order.

2.1. Function Generation

A function generating four-bar mechanism converts a change in input to a change in output correlated by a mathematical function. That is, the output is a desired function of the input. The classical problem of function generation was first formulated trigonometrically by Ferdinand Freudenstein in a seminal paper that has been recognized as the origin of modern kinematics [5]. For a four-bar 4R mechanism the design task becomes identifying the link lengths, which we abstractly define as the *design parameters*, in terms of the constant distances between sequential R-pair centres required to correlate the output link angle, over a prescribed range, as a desired mathematical function of the input angle. In an RRRP linkage the input is still an angle, but the output is a displacement along a line. Function generating mechanisms are found in sewing machines, washing machines, windshield wiper mechanisms, automotive suspensions, aircraft aileron mechanical systems, etc..

2.2. Motion Generation

The design task for motion generation, or rigid body guidance, involves identifying the design parameters of a four-bar mechanism that will guide the coupler through a desired motion. The coupler motion can be defined as the motion of any line on the coupler. Without loss in generality we may consider this as the motion of any coordinate system rigidly attached to the coupler. The motion of the coupler coordinate system consists of the translation of the origin of the coordinate system combined with its change in orientation. Rigid body guidance is also known as the *Burmester problem*, since Ludwig Burmester published the very first recorded work in 1888 outlining a general solution [6]. Motion generating four-bar mechanisms are typically found in aircraft landing gear mechanisms, pick-and-place mechanical systems on automated assembly and packaging conveyors, camera pointing devices, etc..

2.3. Path Generation

Guiding a point along a desired path (curve) is, perhaps, the oldest four-bar linkage problem and was investigated by Archimedes more than two thousand years ago [3] and very likely by many others far earlier. In those times the mechanical devices that generated the desired curve were powered by humans, working animals, or water wheels. This design problem involves identifying the design parameters that will enable a point on the coupler to be guided along a desired curve over a desired range of motion. This point, known as the *coupler point*, is guided along the *coupler point curve* by the motion of the input link and the constraints imposed by the mechanism link lengths. The coupler point can be anywhere on the coupler, and is rarely on the line connecting the centres of the two R-pairs connecting the coupler to the input and output links.

Coupler curves are quite complicated and subtle so we won't dwell on them here. However, it is simple to remember that coupler curves are of degree 6 (sextic) for 4R mechanisms, degree 4 (quartic) for RRRP linkages, and degree 2 (quadratic) for PRRP linkages.

The steam age spawned the *Industrial Revolution* in the 1700s. Coal was needed to boil water to generate the steam that powered the revolution. The need to pump water out of coal mines in England led James Watt to devise a *straight line* linkage that could transfer the oscillating input of a steam power driven piston to a rotating link connected to the piston by a coupler. The concept of the mechanism was patented in 1784 [7]. The coupler was also connected, via an R-pair, to a pumping piston. Thus the power generated by the steam driven piston was transferred to the pumping mechanism which, by design, only needed to do work along the straight line portion of the coupler curve. The Watt linkage, illustrated in Figure 4a, is designed to move point C, located at the midpoint of the coupler, approximately along a straight line over a portion of the curve on which it is constrained to move. This linkage it is still widely used in a large variety of automotive and locomotive suspension systems.

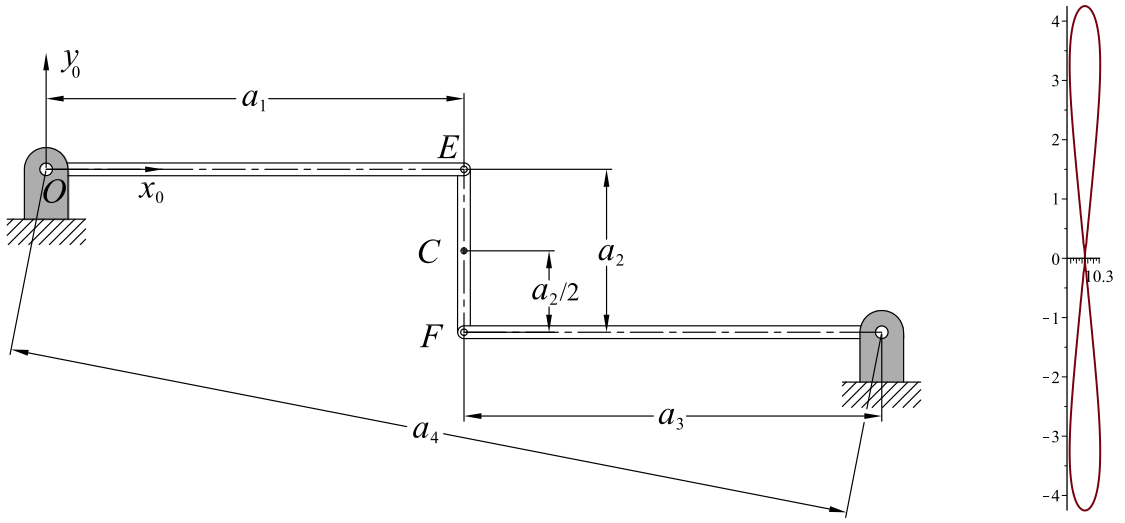

(a) Watt straight line linkage.

(b) Watt coupler curve.

Fig. 4. Watt straight-line linkage and coupler point curve where $a_1 = a_3 = 10$ and $a_2 = 2$.

The link length conditions for an arbitrary Watt mechanism are as follows. The input and output links have the same length, $a_1 = a_3$. The coupler point C is located at $a_2/2$ along the longitudinal centre line of the coupler. The distance between the centres of the two ground-fixed R-pairs can be expressed by the coordinates in the $x_0 - y_0$ coordinate system as $(2a_1,\ a_2)$, and the distance between the two centres is $a_4 = \sqrt{(2a_1)^2 + a_2^2}$. The longest link is always a_4. The coupler point curve for the Watt linkage illustrated in Figure 4a is plotted in Figure 4b.

The mobility constraints on the input and output links are determined by the numerical values of the linear coefficient factors A_1, C_1, and D_1 of Equation (1) are [1]:

$$\begin{aligned} A_1 &= a_1 - a_2 - a_3 + a_4, \\ C_1 &= a_1 - a_2 + a_3 - a_4, \\ D_1 &= a_1 + a_2 - a_3 - a_4. \end{aligned}$$

Because $a_1 = a_3$ and a_4 always represents the longest link length in a Watt mechanism then A_1 is always a positive non-zero number while D_1 is always a negative non-zero number. Moreover, C_1 is always a negative

non-zero number as well since $2a_1 < a_2 + a_4$. Therefore, a Watt straight line mechanism is always a non-Grashof 0-rocker-π-rocker, according to the planar 4R input-output link mobility classification found in [1], and reproduced here as Table 2.

#	A_1	C_1	D_1	Input a_1	Output a_3	#	A_1	C_1	D_1	Input a_1	Output a_3
1	+	+	+	0-rocker	0-rocker	15	0	0	-	crank	π-rocker
2	+	+	0	0-rocker	0-rocker	16	0	-	+	π-rocker	crank
3	+	+	-	rocker	rocker	17	0	-	0	crank	crank
4	+	0	+	0-rocker	crank	18	0	-	-	crank	π-rocker
5	+	0	0	0-rocker	crank	19	-	+	+	crank	crank
6	+	0	-	0-rocker	π-rocker	20	-	+	0	crank	crank
7	+	-	+	rocker	crank	21	-	+	-	π-rocker	π-rocker
8	+	-	0	0-rocker	crank	22	-	0	+	crank	crank
9	+	-	-	0-rocker	π-rocker	23	-	0	0	crank	crank
10	0	+	+	crank	crank	24	-	0	-	crank	π-rocker
11	0	+	0	crank	crank	25	-	-	+	π-rocker	0-rocker
12	0	+	-	π-rocker	π-rocker	26	-	-	0	crank	0-rocker
13	0	0	+	crank	crank	27	-	-	-	crank	rocker
14	0	0	0	crank	crank						

Table 2. Classification of all possible planar 4*R* linkages. Shaded cells satisfy the Grashof condition.

Path generating linkages are now very common in automated manufacturing and assembly operations. Consider an automobile assembly station where windshields are attached to the vehicle body. A uniform bead of adhesive must be applied to the windshield just before a robotic arm picks it up and places it in the precise location on the gasket in the windshield opening on the body. This adhesive is typically applied by a four-bar linkage where the point on the coupler that follows the required adhesive bead path is generated by the input link rotating with constant angular velocity. However, in this case the adhesive bead must be uniform. This means that the coupler point, the nozzle of the adhesive applicator, must also have a constant velocity as it moves along the coupler point curve. Therefore the designer must simultaneously address the position level and velocity level kinematics.

3. PLANAR 4R LINKAGES

The planar 4R four-bar linkage, colloquially known as a *crank-rocker*, *drag-link* (also known as a *double-crank*), or *double-rocker* depending on the link lengths, has been a workhorse in the realm of mechanical and aerospace engineering for centuries, if not millennia [3]. While trigonometric analytical methods to study the relationship between the motions of the input and output links, based on the distances between the R-pair centres have existed for at least 150 years [8], purely algebraic methods have not. This means that the theory of algebraic differential geometry [9, 10] cannot be used to identify the structure of the relationship between the input and output parameters. Still, trigonometric methods are highly accessible and largely intuitive. The trigonometric input-output (IO) equations for planar 4R linkages that have become the backbone of analysis and synthesis were first introduced by Ferdinand Freudenstein in the 1950s [5, 11]. The same trigonometric approach has been used for planar RRRP linkages as well as for those containing as many as two P-pairs [2].

The algebraic IO equation for a planar 4R linkage is an algebraic polynomial that relates the tangent half-angle parameter of the input joint angle to the tangent half-angle parameter of the output joint angle in terms

of the link lengths [12, 13]. A polynomial is algebraic if the coefficients are rational numbers[2]. This IO equation can be derived algorithmically [14] without explicit reference to trigonometry using the Denavit-Hartenberg (DH) parametrisation of the linkage kinematic geometry [15], Study's kinematic mapping [16], and Gröbner bases [17, 18]. Algebraic IO equations for any closed RRRP and PRRP kinematic chain can be similarly derived from the kinematic geometry but, as it turns out, this is unnecessary. Recent work by Rotzoll et al. [14, 19] has yielded the remarkable result that the algebraic IO equations for planar four-bar linkages that contain one, two, three, or even four P-pairs are embedded in the general planar 4R algebraic IO equation. That is, one need only collect the planar 4R algebraic IO equation in terms of the variable input and output parameters. Regardless, these algebraic IO equations can be derived from the kinematic geometry. The interested reader is referred to [20] for details.

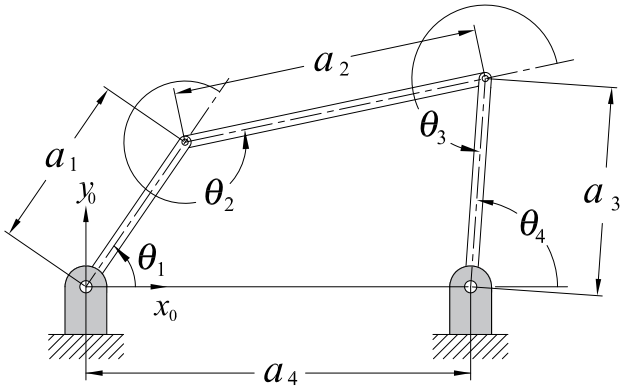

Fig. 5. Planar 4R closed kinematic chain.

Consider the planar 4R closed kinematic chain illustrated in Figure 5. The basis vector directions of the non-moving coordinate reference system are x_0-y_0. The coordinate system origin is located at the rotation centre of the input link ground-fixed R-pair, while the x_0-axis points towards the rotation centre of that of the output link. The algebraic IO equation of an arbitrary planar 4R linkage illustrated in Figure 5 is represented as

$$Av_1^2v_4^2 + Bv_1^2 + Cv_4^2 - 8a_1a_3v_1v_4 + D = 0, \tag{1}$$

where

$$\begin{aligned}
A &= (a_1 - a_2 - a_3 + a_4)(a_1 + a_2 - a_3 + a_4) = A_1A_2;\\
B &= (a_1 - a_2 + a_3 + a_4)(a_1 + a_2 + a_3 + a_4) = B_1B_2;\\
C &= (a_1 - a_2 + a_3 - a_4)(a_1 + a_2 + a_3 - a_4) = C_1C_2;\\
D &= (a_1 + a_2 - a_3 - a_4)(a_1 - a_2 - a_3 - a_4) = D_1D_2;\\
v_1 &= \tan\left(\frac{\theta_1}{2}\right); \quad v_4 = \tan\left(\frac{\theta_4}{2}\right).
\end{aligned}$$

The joint angle parameters v_1 and v_4 represent the tangent half-angles of linkage input and output angles, θ_1 and θ_4. The eight bilinear factors of the coefficients A, B, C, and D in Equation (1) depend on the numerical values of the four a_i link lengths. In this formulation the input link, a_1, is always positive but the remaining three a_i directed distances are the unique eight permutations of positive and negative signs in each factor. Hence, the eight bilinear factors represent eight distinct planes. Note that these permutations in sign only

[2]A rational number can be expressed exactly as the ratio of two integers. The number $3.333\cdots$ is rational because it can be expressed exactly by the ratio 1/3, whereas the number $\sqrt{2}$ is irrational because it cannot be expressed exactly by such a ratio.

applies to the arithmetic operations of addition and subtraction, they do not represent the sign of the numeric value of the directed length. Treating the four a_i as homogeneous coordinates with a_4 as the homogenising coordinate one can uniformly scale the numerical values of the four a_i by dividing by a_4, which is always an arbitrary nonzero number for any real 4R linkage, without affecting the functional relationship $v_4 = f(v_1)$. Treating the a_i as mutually orthogonal basis directions in the hyperplane $a_4 = 1$, the eight planes intersect in the only uniform polyhedral compound [21], called the stellated octahedron, which has order 48 octahedral symmetry: a regular double tetrahedron that intersects itself in a regular octahedron [22]. The location of a point in this space completely determines the relative mobility of all four links and hence it is termed the *design parameter space* of planar 4R linkages.

There has always existed an almost innate understanding that as the radius of a sphere tends towards infinity it can be considered as the plane at infinity. Projective geometry has, of course, shown that this is indeed the case mathematically [23]. The axes of a spherical 4R linkage intersect at the centre of the sphere, see the spherical 4R illustrated in Figure 6b, while those of a planar 4R are mutually parallel but intersect in a unique point on the line at infinity in the projective extension of the Euclidean plane of the 4R mechanism. Therefore, there arose the notion in the 1800's that planar 4R mechanisms are special cases of spherical 4R linkages on the surface of a sphere of infinite radius. This notion was proved to be true in [24] and more recently in [14] where the proof is relatively straightforward using the algebraic form of the IO equation.

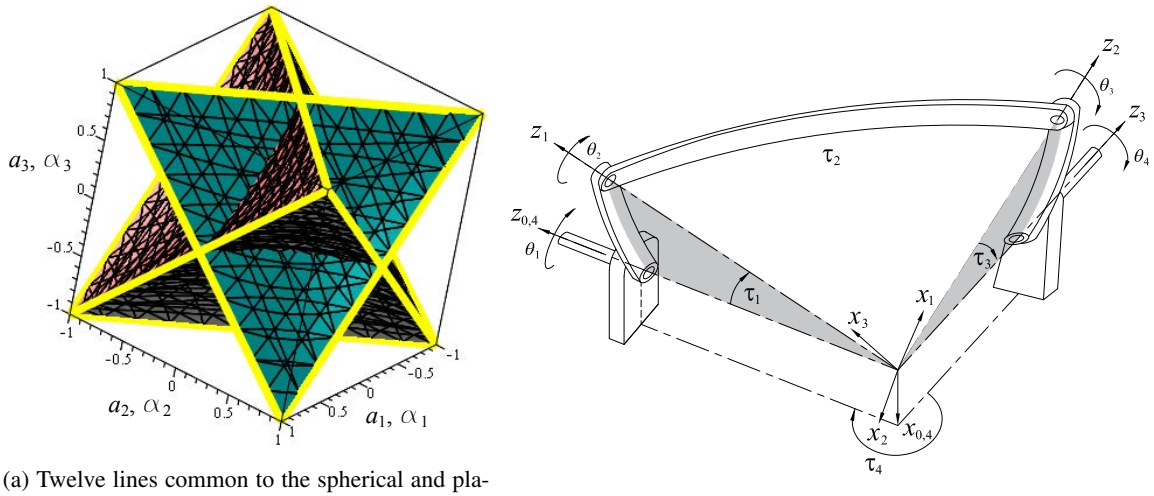

(a) Twelve lines common to the spherical and planar 4R design parameter spaces.

(b) A spherical 4R mechanism.

Fig. 6. Design parameter space intersections and a planar RRRP linkage.

The design parameters of a spherical 4R are four nonzero arc length angle parameters, which are the tangent half-angle parameters, α_i, of the arc length angles, τ_i, such that $\alpha_i = \tan(\tau_i/2)$. The algebraic IO equation of a spherical 4R contains eight bicubic factors in the α_i. These eight cubic factors are singular cubic surfaces [21] in the sense that they all contain only 12 and not the maximum number of 27 lines [25]. Each cubic surface contains three real finite lines which intersect in an equilateral triangle and different pairs of the eight cubic surfaces have a different line in common. Treating the four α_i as mutually orthogonal basis directions and projecting into the hyperplane $\alpha_4 = 1$ reveals the design parameter space of spherical 4R linkages. Each distinct point in this space is a unique spherical 4R and the mobility of the input and output links is completely determined by its location in this space. It turns out that the eight cubic surfaces in the spherical 4R design parameter space intersect the planar 4R design parameter space in the 12 edges of the double tetrahedra, see Figure 6a. The vertices of the tetrahedra are the vertices of the equilateral triangles on each cubic surface while the edges are the lines themselves.

3.1. Planar 4R Algebraic IO Equations

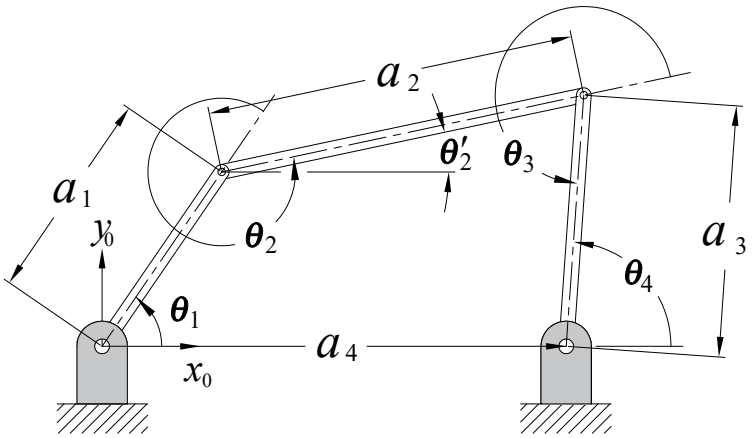

Fig. 7. Planar 4R Joint Angles.

Consider the planar 4R linkage illustrated in Figure 7. The standard variables are the a_1 and a_3 joint angles θ_1 and θ_4. But we can choose any pair of links to act as "input" and as "output" meaning that there are five additional IO pairings, in addition to Equation (1), reprinted here as Equation (2) for convenience. The six possible algebraic IO equations are [26]:

$$Av_1^2v_4^2 + Bv_1^2 + Cv_4^2 - 8a_1a_3v_1v_4 + D = 0, \tag{2}$$

where

$$\begin{gathered}
A = A_1A_2 = (a_1 - a_2 - a_3 + a_4)(a_1 + a_2 - a_3 + a_4),\\
B = B_1B_2 = (a_1 - a_2 + a_3 + a_4)(a_1 + a_2 + a_3 + a_4),\\
C = C_1C_2 = (a_1 - a_2 + a_3 - a_4)(a_1 + a_2 + a_3 - a_4),\\
D = D_1D_2 = (a_1 + a_2 - a_3 - a_4)(a_1 - a_2 - a_3 - a_4),\\
v_1 = \tan\tfrac{\theta_1}{2},\\
v_4 = \tan\tfrac{\theta_4}{2};
\end{gathered}$$

the five other algebraic IO equations are

$$A_1B_1v_1^2v_2^2 + A_2B_2v_1^2 + C_1D_2v_2^2 + 8a_2a_4v_1v_2 + C_2D_1 = 0; \tag{3}$$

$$A_2B_1v_1^2v_3^2 + A_1B_2v_1^2 + C_1D_1v_3^2 + C_2D_2 = 0; \tag{4}$$

$$B_1C_1v_2^2v_3^2 + A_1D_2v_2^2 + A_2D_1v_3^2 - 8a_1a_3v_2v_3 + B_2C_2 = 0; \tag{5}$$

$$A_1C_1v_2^2v_4^2 + B_1D_2v_2^2 + A_2C_2v_4^2 + B_2D_1 = 0; \tag{6}$$

$$A_2C_1v_3^2v_4^2 + B_1D_1v_3^2 + A_1C_2v_4^2 - 8a_2a_4v_3v_4 + B_2D_2 = 0. \tag{7}$$

3.1.1. v_i-v_j Input-output Curves

Consider a planar 4R linkage where $a_1 = 2$, $a_2 = 6$, $a_3 = 8$, $a_4 = 5$ in generic units of length. Substituting these link lengths into Equation (2) yields:

$$-35v_1^2v_4^2 + 189v_1^2 - 128v_1v_4 - 11v_4^2 + 85 \quad = \quad 0.$$

Making an implicit plot in Maple reveals the $v1$-$v4$ curve over a specified range of bounding values for the two numbers defined by $\tan(\theta_i/2)$ illustrates the curves in each assembly mode. The implicit plot command works by evaluating a number of points on the curve that you can specify, then solving the equation for v_4 for each incremental value of v_1. However, the v_1-v_4 IO curves illustrated in Figure 8 were created with GeoGebra to show both the coupler point and IO curves. Substituting the link lengths into the remaining five v_i-v_j IO equations (3) through (7) reveal the functional correlation between the specified pair of joint angle parameters in Figures 9 through 11.

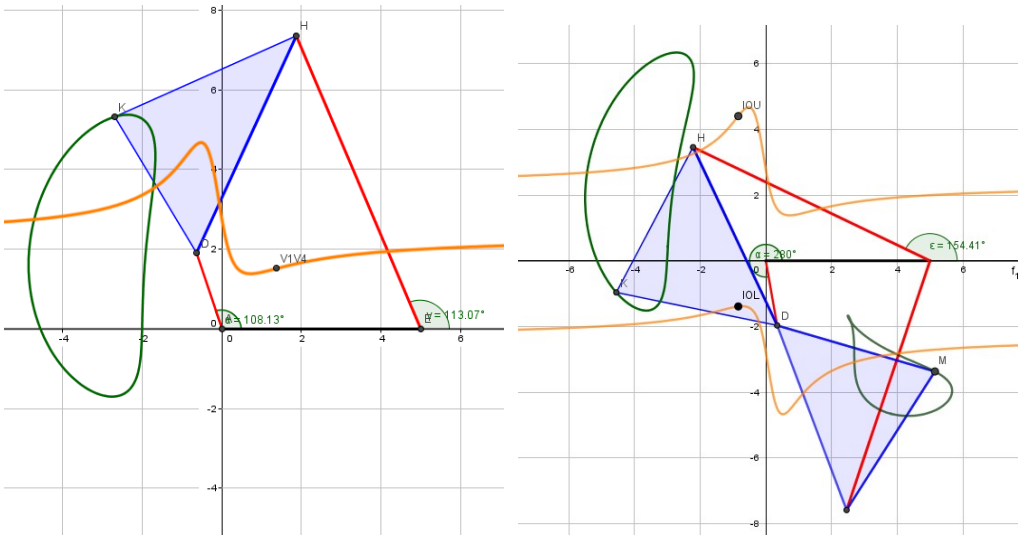

(a) v_1-v_4 IO and coupler curves, upper assembly mode.

(b) v_1-v_4 IO and coupler curves, both assembly modes.

Fig. 8. Planar 4R v_1-v_4 IO and coupler curves for $a_1 = 2$, $a_2 = 6$, $a_3 = 8$, and $a_4 = 5$.

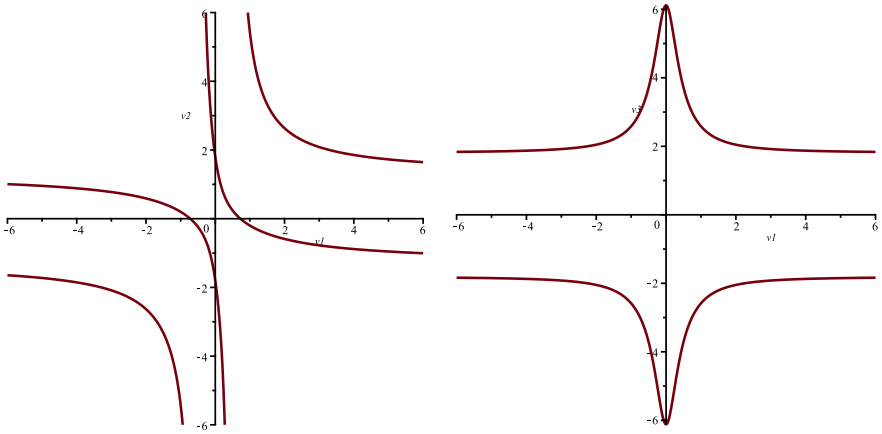

Fig. 9. Planar 4R v_1-v_2 and v_1-v_3 IO curves for $a_1 = 2$, $a_2 = 6$, $a_3 = 8$, and $a_4 = 5$.

Examining the figures, we can immediately deduce the relative angular displacement ranges between the associated joint angle parameter pairs. Figure 8 indicates that Link a_1 is a crank and a_3 is a rocker, both relative to a_4. Figures 9 indicate that a_1 is a crank relative to a_4 while a_2 is also a crank relative to a_1 for the v_1-v_2 IO curve and a_1 is a crank relative to a_4 while a_3 is a rocker relative to a_1 for the v_1-v_3 IO curve.

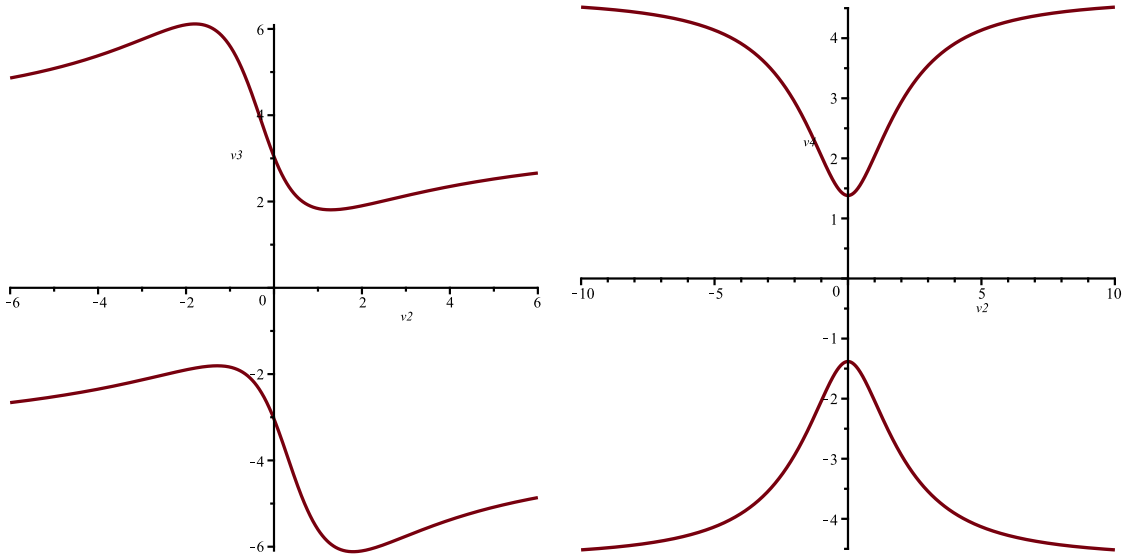

Fig. 10. Planar 4R v_2-v_3 and v_2-v_4 IO curves for $a_1 = 2$, $a_2 = 6$, $a_3 = 8$, and $a_4 = 5$.

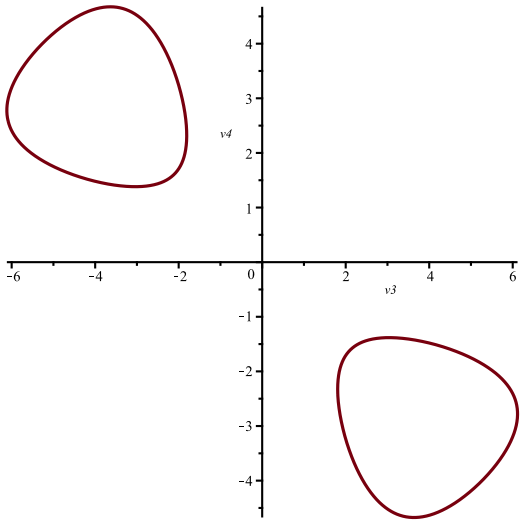

Fig. 11. Planar 4R v_3-v_4 IO curve for $a_1 = 2$, $a_2 = 6$, $a_3 = 8$, and $a_4 = 5$.

Figures 10 indicate that a_2 is a crank relative to a_1 while a_3 is rocker relative to a_2 for the v_2-v_3 IO curve and a_2 is a crank relative to a_1 while a_4 is a rocker relative to a_3 for the v_2-v_4 IO curve. Lastly, Figure 11 reveals that a_3 is a rocker relative to a_4 while a_4 is rocker relative to a_3 for the v_3-v_4 IO curve.

3.2. Mobility Classification

The double points at infinity belonging to each of the four distinct v_i coordinate axes together with the type of points at $v_i = 0$ completely define the mobility limits, if they exist, between each v_i-v_j angle parameter pair. Physically speaking, these two points correspond to the two extreme orientations implied by the v_i where the two links can align. Hence, the examination of these two points is sufficient to determine whether a particular joint enables a crank, a rocker, a π-rocker, or a 0-rocker link motion [1]. This may help clarify some of the terms found in Table 2.

3.2.1. Double Points

Before examining the classification, *double points* require some discussion. Each point of each distinct branch of an algebraic curve possesses at least one distinct tangent. What happens if the curve does not possess distinct branches or if the curve self-intersects? If a curve intersects itself then there must be more than one tangent to the curve at the self-intersection location. How can a point of the curve that possesses two, or more, tangents be classified? In the study of the kinematic geometry of mechanisms [27], and of algebraic differential geometry in general [9, 10], these special locations have important meanings for linkage velocities, accelerations, and jerks. These locations are usually called *multiple points* because there are multiple tangents at that point. They are also called *singular points* because the point is uniquely defined at that location, and hence *singular*. However, work with planar four-bar linkages requires only knowledge of *double points*, locations where a curve intersects itself a single time. A comprehensive account of multiple points can be found in [28] for the interested reader.

There are three species of double point that arise when the tangents to the curve at the double point are either a pair of distinct real lines, a pair of complex conjugate lines, or a pair of real but coincident lines. Methods to analytically identify the presence of double points of an algebraic curve and to determine the class of the double point are discussed next. The type of double point can be used to classify the mobility capability of input link.

To illustrate the different nature of the three types of double point consider the following cubic equation

$$y^2 \quad = \quad (x-a)(x-b)(x-c) \tag{8}$$

where the constant coefficients have rational positive magnitudes such that $a < b < c$. This curve, illustrated in Figure 12a, is symmetric with respect to the x-axis since every value of x gives equal and opposite values of y. The curve intersects the x-axis at the three points $x = a$, $x = b$, and $x = c$. When $x < a$ the value of y^2 is negative, and y is imaginary. When $a < x < b$ then y^2 is positive, and there are two real, equal and opposite values for y. For values of $b < x < c$ the value for y^2 is again negative, and finally positive again for all values $x > c$. The curve therefore consists of a closed oval between a and b and an open branch beginning at c and extending infinitely in two directions beyond it. The curve illustrated in Figure 12a has $a = 2$, $b = 4$, and $c = 5$. These values will now be manipulated to yield examples of the three types of double point.

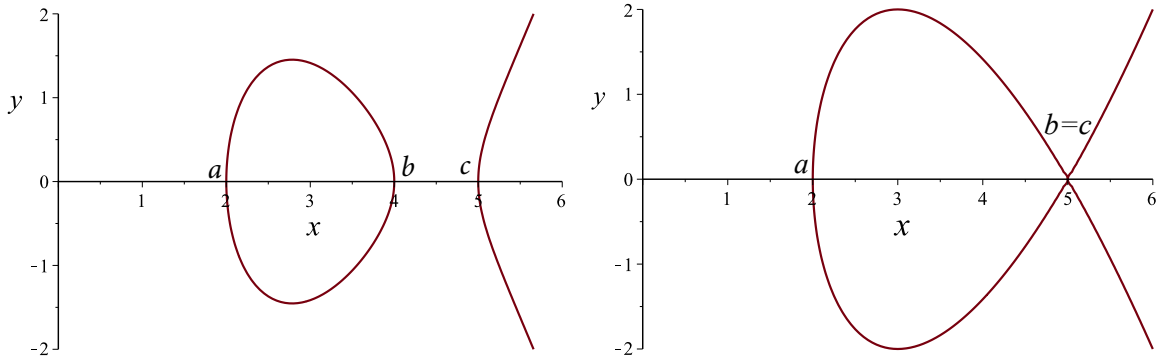

(a) Cubic with two real branches and no double points.

(b) A *regular double point*, or crunode.

Fig. 12. Species of double points: *regular*.

Expanding Equation (8) and collecting the terms in descending powers of x and y leads to a polynomial equation, $f(x,y) = 0$:

$$f(x,y) := \quad x^3 - (a+b+c)x^2 + (ab+ac+bc)x - y^2 - abc \quad = \quad 0. \tag{9}$$

Let b vary in magnitude between the range $a \leq b \leq c$. As b increases in value the oval circuit increases in size maintaining it's location at a but growing towards c until $b = c$ and the curve crosses itself. In this example $a = 2$ and $b = c = 5$. Inspecting the curve illustrated in Figure 12b we see that at the double point, or node, the two branches of the curve meet, and each branch has it's own real, distinct tangent. Such a point is called a *regular double point*, or a *crunode*. There is only one common zero of Equation (9) and it's partial derivatives with respect to x and y: $(x,y) = (5,0)$. The discriminant of Equation (9) given by Equation (14) is

$$\Delta \quad = \quad 12x - 48. \tag{10}$$

Evaluating Equation (10) at the double point $(x,y) = (5,0)$ leads to

$$\Delta \quad = \quad 12 \; > \; 0,$$

which is a positive non-zero number, as it must be, since the multiple point is a regular double point, or crunode.

As b moves in the opposite direction towards a, the original oval circuit in Figure 12a now shrinks in size until $b = a$, giving for $a = b = 2$ and $c = 5$

$$x^3 - 9x^2 + 24x - y^2 - 20 \quad = \quad 0. \tag{11}$$

as illustrated in Figure 13a. The cubic now possesses an *isolated double point* at $x = a = b = 2$. Isolated double points, also known as *acnodes* or *hermit points*, satisfy the equation of the cubic but do not appear to lie on the curve. The tangents to the curve at an isolated double point are a pair of complex conjugate lines. No real line through the isolated double point intersects the curve in more than two real points, confirming the necessary condition that a general real line cuts a cubic in three points. The reader should confirm that the common solution to Equation (11) and it's partial derivatives with respect to x and y is $(x,y) = (2,0)$, and that the discriminant of Equation (11) evaluated at the double point is

$$\Delta \quad = \quad -12 \; < \; 0.$$

The result is a number less than zero, as it must be, since this is an isolated double point, or acnode.

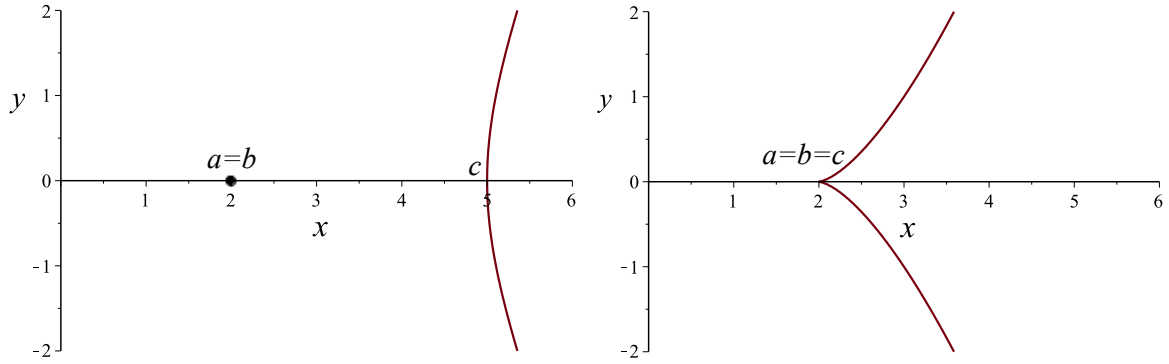

(a) An *isolated double point*, or acnode, or hermit point. (b) A *stationary double point*, or spinode , or cusp.

Fig. 13. Species of double points: *isolated* and *stationary*.

The third species of double point occurs if the equation of the tangent to the curve at a point becomes a perfect square. In this case the tangents at the self-intersection point, called a *stationary double point* are

two real, but coincident lines. In the case of the cubic in Equation (8), if we allow both coefficients b and c to approach a then the two distinct branches of the curve merge into a single branch when $a = b = c$ and Equation (8) becomes

$$y^2 \quad = (x-a)^3. \tag{12}$$

When expanded and collected in terms of descending powers of x and y then Equation (12) can be expressed as the polynomial equation for $a = b = c = 2$

$$x^3 - 6x^2 + 12x - y^2 - 8 \quad = \quad 0. \tag{13}$$

This situation is illustrated in Figure 13b. The stationary double point where $x = a = b = c$ is also called a *cusp* or a *spinode*. They are called stationary double points because if the curve is generated by the motion of a point then at a cusp the motion of the point in one direction comes to a stop and changes direction making the velocity of the point instantaneously zero at the stationary double point coordinates. The tangent at the cusp meets the curve in three coincident points at $(a,0)$ in Figure 13b. The reader should confirm that the common solution to Equation (13) and it's partial derivatives with respect to x and y is $(x,y) = (2,0)$, and that the discriminant of Equation (13) evaluated at the double point is

$$\Delta \quad = \quad 0.$$

The differential geometry implied by the discriminant demands that it's value, evaluated at the stationary double point $(x,y) = (2,0)$, is identically equal to zero.

3.2.2. Homogeneous Coordinates

Let O be the origin of the Cartesian coordinate system, shown in Figure 14. Let S be a distinct point in the plane. The ray passing through O and S is described by the coordinate pair (x,y). Another distinct point $Q \neq O$, on ray OS is described by the pair $(\mu x, \mu y)$, where $\mu \in \mathbb{R}$ (ie., a real number). As $\mu \to \pm\infty$ the seemingly meaningless pair (∞,∞) is obtained [29].

To remedy this representational problem, the point pairs may be represented by two ratios, given by ordered triples (x_0, x_1, x_2). If $x_0 \neq 0$, then the point S can be uniquely described as:

$$x = \frac{x_1}{x_0}, \;\; y = \frac{x_2}{x_0}.$$

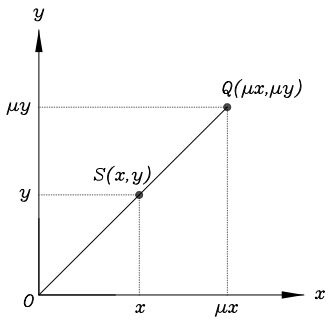

Fig. 14. Cartesian coordinates in E_2.

Then any triple of the form $(\lambda x_0, \lambda x_1, \lambda x_2)$, for $\lambda \neq 0$, describes exactly the same point S. In other words, two real points are equal if the triples representing them are proportional. This is because

$$\frac{\lambda x_1}{\lambda x_0} = \frac{x_1}{x_0} = x, \quad \text{and} \quad \frac{\lambda x_2}{\lambda x_0} = y.$$

The corresponding coordinates $(x_0 : x_1 : x_2)$ are called *homogeneous coordinates*, but are really three ratios. This is indicated with the symbol : in the set of homogeneous coordinates. When $x_0 = 1$ the Cartesian coordinate pair (x,y) is recovered.

3.2.3. Mobility Classification Conditions

One possibility to determine the type of double point, i.e., whether it is a crunode, acnode, or cusp, is to evaluate whether the double point has a pair of real, or complex conjugate tangents. If the double point has two real distinct tangents, it is a crunode; if it has two real coincident tangents, it is a cusp; and if the tangents are both complex conjugates, the double point is an acnode [9, 30]. Thus, after homogenising each v_i-v_j angle pair IO equation using the homogenising coordinate v_0, leading to IO_h, the following discriminant yields information on the double point at infinity on the v_j axis:

$$\Delta = \left(\frac{\partial^2 IO_h}{\partial v_i \partial v_0}\right)^2 - \frac{\partial^2 IO_h}{\partial v_i^2}\frac{\partial^2 IO_h}{\partial v_0^2} \begin{cases} > 0 \Rightarrow \text{crunode;} \\ = 0 \Rightarrow \text{cusp;} \\ < 0 \Rightarrow \text{acnode.} \end{cases} \tag{14}$$

To obtain, for example, the homogeneous v_1-v_4 IO equation of an arbitrary planar 4R linkage we must redefine the (v_1, v_4) coordinates as three homogeneous ratios. The discriminant of the point at infinity $(v_0 : v_1 : v_4) = (0 : 1 : 0)$ on the v_1-axis is obtained by setting $i = 4$ in the discriminant equation, i.e. ∂v_4, while the discriminant of the other point at infinity $(v_0 : v_1 : v_4) = (0 : 0 : 1)$ on the v_4-axis is obtained by setting i = 1 in the discriminant equation, i.e. ∂v_1.

Proceeding with the double point analysis of all six v_i-v_j equations at infinity on both axes results in 12 discriminants. However, as the v_i-v_j equations are all dependent on each other, from the 12 discriminants we are left with only four distinct ones describing the nature of the double points at infinity of each v_i for $i \in \{1...4\}$. The complete derivation can be found in [26], but in that paper different coordinate systems are used meaning that the coefficients have different definition from those defined in this tutorial in Equation (2).

Using the coordinate system definitions observed in Figure 5 it can be shown that the conditions on the angular mobility of one of the four links, relative to the link with respect to which the angle is measured, are listed in Tables 3-6, where the eight bilinear factors A_1-D_2 are defined in Equation (2). This approach to the angular mobility classification of the individual links provides an arguably more general set of conditions than those found in Table 2.

Table 3. Mobility of a_1 relative to a_4.

$C_1C_2D_1D_2$	$A_1A_2B_1B_2$	mobility of a_1
≤ 0	≤ 0	crank
≤ 0	> 0	0-rocker
> 0	≤ 0	π-rocker
> 0	> 0	rocker

Table 4. Mobility of a_2 relative to a_1.

$A_1B_1C_1D_2$	$A_2B_2C_2D_1$	mobility of a_2
≤ 0	≤ 0	crank
≤ 0	> 0	π-rocker
> 0	≤ 0	0-rocker
> 0	> 0	rocker

Table 5. Mobility of a_3 relative to a_2.

$A_2B_1C_1D_1$	$A_1B_2C_2D_2$	mobility of a_3
≤ 0	≤ 0	crank
≤ 0	> 0	π-rocker
> 0	≤ 0	0-rocker
> 0	> 0	rocker

Table 6. Mobility of a_3 relative to a_4.

$A_1A_2C_1C_2$	$B_1B_2D_1D_2$	mobility of a_3
≤ 0	≤ 0	crank
≤ 0	> 0	π-rocker
> 0	≤ 0	0-rocker
> 0	> 0	rocker

3.2.4. Computing Critical Input Angles to Determine Output Angle Extreme Values

If the mobility classification reveals that angular displacement limits exist for a link in a planar 4R mechanism, how can the numerical values of the limits be computed? This task is efficiently accomplished using differential calculus. Consider the mobility limits for the 4R linkage IO curve illustrated in Figure 8b where

$a_1 = 2$, $a_2 = 6$, $a_3 = 8$, and $a_4 = 5$. The v_1-v_4 algebraic IO equation for these link lengths is reproduced here for convenience:

$$-35v_1^2v_4^2 + 189v_1^2 - 128v_1v_4 - 11v_4^2 + 85 = 0. \tag{15}$$

To determine the angle parameter limits between which the output link a_3 rocks in each assembly mode requires the critical values $v_{1_{\text{crit}}}$ at which the limiting values of v_4 occur. First solve Equation (15) for v_4:

$$v_4 = \frac{-64v_1 \pm \sqrt{615v_1^4 + 9150v_1^2 + 935}}{35v_1^2 + 11}. \tag{16}$$

Each solution in Equation (16) represents the value of v_4 for a specified value of v_1 in each assembly mode. To determine the two values of $v_{1_{\text{crit}}}$ in each assembly mode, the derivative of Equation (16) must be taken with respect to v_1. Solve the resulting derivatives for $v_{1_{\text{crit}}}$ that satisfy

$$\frac{dv_4}{dv_1} = 0. \tag{17}$$

In this example, we find for one assembly mode that

$$v_{1_{\text{crit}}} = \frac{\sqrt{231}}{21} \text{ and, } -\frac{\sqrt{119}}{21}, \tag{18}$$

while for the other assembly mode we find

$$v_{1_{\text{crit}}} = -\frac{\sqrt{231}}{21} \text{ and, } \frac{\sqrt{119}}{21}. \tag{19}$$

Substituting each value for $v_{1_{\text{crit}}}$ into Equation (16) reveals the corresponding extreme values for v_4, listed in Table 7. The angle equivalents for $\theta_{1_{\text{crit}}}$ and $\theta_{4_{\text{min/max}}}$ are listed in Table 8. Figures 15 and 16 illustrate the linkage in its extreme configurations in each assembly mode.

Table 7. $v_{4_{\text{min/max}}}$.

v_4	Assembly Mode 1	Assembly Mode 2
$v_{4_{\text{min}}}$	1.381698560	-1.381698560
$v_{4_{\text{max}}}$	4.675162334	-4.675162334

Table 8. $\theta_{1_{\text{crit}}}$ and $\theta_{4_{\text{min/max}}}$.

	Assembly Mode 1	Assembly Mode 2		Assembly Mode 1	Assembly Mode 2
$\theta_{1_{\text{crit}}}$	71.79004310°	54.90036778°	$\theta_{4_{\text{min/max}}}$	108.2099569°	-155.85315208°
	-54.90036778°	-71.79004310°		155.85315208°	-108.2099569°

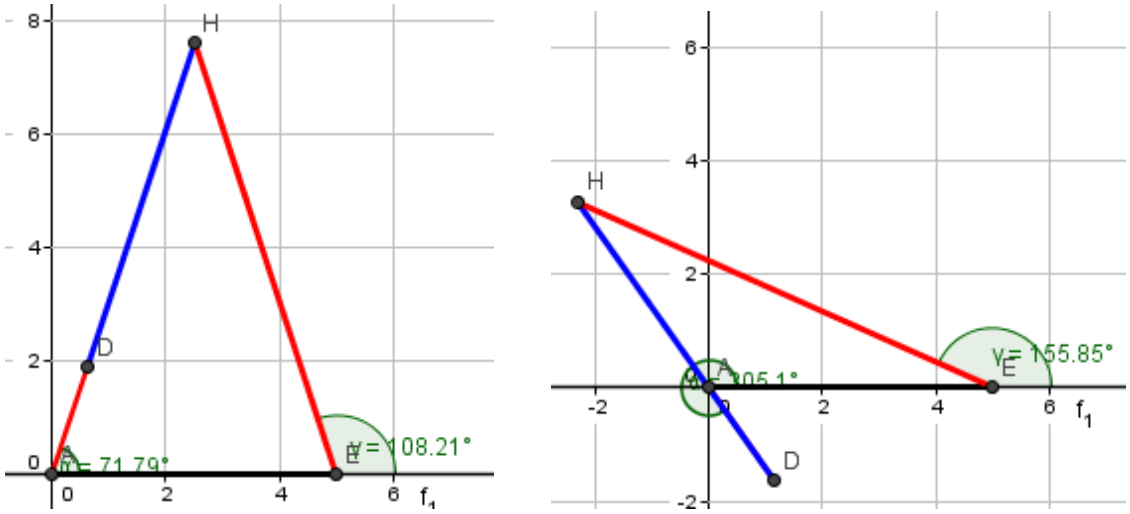

(a) Configuration for $\theta_{4_{\min}}$.

(b) Configuration for $\theta_{4_{\max}}$

Fig. 15. Assembly Mode 1 $\theta_{1_{\text{crit}}}$ and $\theta_{4_{\min/\max}}$.

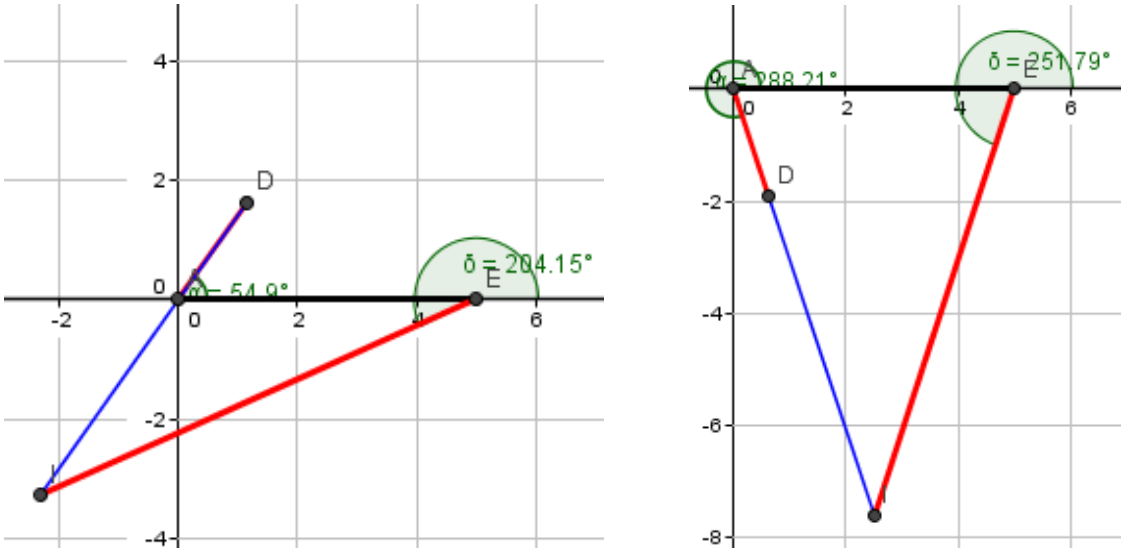

(a) Configuration for $\theta_{4_{\min}}$.

(b) Configuration for $\theta_{4_{\max}}$

Fig. 16. Assembly Mode 2 $\theta_{1_{\text{crit}}}$ and $\theta_{4_{\min/\max}}$.

3.3. Planar 4R Algebraic Angular Velocity IO Equations

The equation relating the time rates of change of the joint angle parameters v_1 and v_4 can be determined as the first time derivative of Equation (2):

$$\big((Av_4^2+B)v_1-4a_1a_3v_4\big)\dot{v}_1+\big((Av_1^2+C)v_4-4a_1a_3v_1\big)\dot{v}_4. \tag{20}$$

Because Equation (20) equates to zero, the velocity parameter ratio can be expressed as

$$\frac{\dot{v}_4}{\dot{v}_1} = -\frac{(Av_4^2+B)v_1-4a_1a_3v_4}{(Av_1^2+C)v_4-4a_1a_3v_1}, \tag{21}$$

which can also be directly obtained as the implicit derivatives of Equation (2) with respect to v_1 and v_4. It is important to note that for the i^{th} link, $\dot{v}_i \neq \dot{\theta}_i$ since $v_i = \tan(\theta_i/2)$. But it is a simple matter to show that

$$\dot{v}_i = \frac{\dot{\theta}_i(1+v_i^2)}{2}, \tag{22}$$

and that

$$\dot{\theta}_i = \frac{2\dot{v}_i}{(1+v_i^2)}. \tag{23}$$

Hence, the reciprocal of the mechanical advantage is

$$\frac{\dot{\theta}_4}{\dot{\theta}_1} = -\frac{((Av_4^2+B)v_1 - 4a_1a_3v_4)(1+v_1^2)}{((Av_1^2+C)v_4 - 4a_1a_3v_1)(1+v_4^2)}. \tag{24}$$

The remaining angular velocity equations are expressed as the following ratios

$$\frac{\dot{\theta}_2}{\dot{\theta}_1} = -\frac{((A_1B_1v_2^2+A_2B_2)v_1 + 4a_2a_4v_2)(1+v_1^2)}{((A_1B_1v_1^2+C_1D_2)v_2 + 4a_2a_4v_1)(1+v_2^2)}, \tag{25}$$

$$\frac{\dot{\theta}_3}{\dot{\theta}_1} = -\frac{((A_2B_1v_3^2+A_1B_2)v_1)(1+v_1^2)}{((A_2B_1v_1^2+C_1D_1)v_3)(1+v_3^2)}, \tag{26}$$

$$\frac{\dot{\theta}_3}{\dot{\theta}_2} = -\frac{((B_1C_1v_3^2+A_1D_2)v_2 - 4a_2a_4v_3)(1+v_2^2)}{((B_1C_1v_2^2+A_2D_1)v_3 - 4a_2a_4v_2)(1+v_3^2)}, \tag{27}$$

$$\frac{\dot{\theta}_4}{\dot{\theta}_2} = -\frac{((A_1C_1v_4^2+B_1D_2)v_2)(1+v_2^2)}{((A_1C_1v_2^2+A_2C_2)v_4)(1+v_4^2)}, \tag{28}$$

$$\frac{\dot{\theta}_4}{\dot{\theta}_3} = -\frac{((A_2C_1v_4^2+B_1D_1)v_3 - 4a_2a_4v_4)(1+v_3^2)}{((A_2C_1v_3^2+A_1C_2)v_4 - 4a_2a_4v_3)(1+v_4^2)}, \tag{29}$$

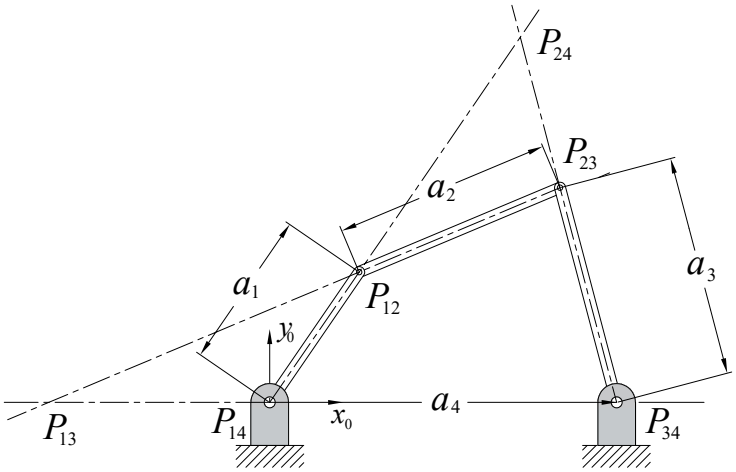

Fig. 17. The six instantaneous centres of velocity.

3.4. Generalisation of Freudenstein's Theorem 1

Consider the planar 4R linkage illustrated in Figure 17. It is well known that as the 4R linkage moves it has four primary instantaneous centres of velocity (ICV), one at the centre of each R-pair. Two of the primary ICVs, P_{12} and P_{23}, move on centrodes defined by the link lengths, while P_{14} and P_{34} are stationary. The two secondary ICVs are P_{13} and P_{24}, which also move on centrodes. By virtue of the Aronhold-Kennedy theorem, P_{13}, P_{14}, and P_{34} remain collinear as the motion evolves over time meaning that the centrode for P_{13} is the line joining the two ground-fixed R-pairs, the x_0-axis, and is located at the point of intersection of the x_0-axis and the extension of the centreline of the coupler, a_2. Freudenstein's Theorem 1 [31, 32] states that the value of the ratio of the output angular velocity and the input angular velocity, $\dot{\theta}_4$ and $\dot{\theta}_1$, can be expressed by the ratio of the values of the relative directed distances between the three ICVs located on the x_0-axis in the following way:

$$\frac{\dot{\theta}_4}{\dot{\theta}_1} = \frac{d_{P_{13}P_{14}}}{d_{P_{13}P_{14}} + d_{P_{14}P_{34}}}, \tag{30}$$

where the directed distances $d_{P_{14}P_{34}}$ and $d_{P_{13}P_{14}}$ can be positive or negative depending on their relative directions.

It is a straightforward computation to express the value of the location of P_{13} as the point of intersection of the longitudinal centreline of the coupler and the line containing the x_0-axis in terms of the link directed lengths and the joint angle parameters v_1 and v_4 as

$$\frac{\left(\frac{a_1(a_3v_1^2v_4 - a_3v_1v_4^2 + a_4v_1v_4^2 + a_3v_1 - a_3v_4 + a_4v_1)}{a_1v_1v_4^2 - a_3v_1^2v_4 + a_1v_1 - a_3v_4}\right)}{\left(\frac{a_1(a_3v_1^2v_4 - a_3v_1v_4^2 + a_4v_1v_4^2 + a_3v_1 - a_3v_4 + a_4v_1)}{a_1v_1v_4^2 - a_3v_1^2v_4 + a_1v_1 - a_3v_4} + a_4\right)}. \tag{31}$$

Selecting a configuration of a viable planar 4R and substituting the appropriate values it is a simple matter to show that the values of Equations (24), (30), and (31) are equivalent. For example, substituting the a_i values of $a_1 = 7$, $a_2 = 13$, $a_3 = 8$, $a_4 = 16$, $v_1 = \tan(60/2)$ and $v_4 = \tan(87.4498/2)$ into the three equations leads to the identical result

$$\frac{\dot{v}_4(1+v_1^2)}{\dot{v}_1(1+v_4^2)} = 0.6974. \tag{32}$$

However, Freudenstein's first theorem also applies to the ICVs on each of the three other Aronhold-Kennedy lines of three collinear ICVs with respect to a number line coincident with the line of three ICVs having its

Table 9. Configuration parameters for a closed 4R chain.

Parameter	Dimension	Parameter	Dimension
a_1	5	$d_{P_{13}P_{14}}$	-32.4571
a_2	6	$d_{P_{13}P_{12}}$	-29.1205
a_3	8	$d_{P_{24}P_{12}}$	6.6954
a_4	2	$d_{P_{24}P_{23}}$	11.4161
θ_1	45°	θ_3	207.5141°
θ_2	308.0304°	θ_4	20.5445°

origin on the central ICV. It seems that, to the best of the authors collective knowledge, this fact has never been discussed in the literature. The six ICVs are known as *velocity poles* and the curves they move along are described as *polodes*, see [2, 4, 33, 34] for example. However, it seems that the following three velocity ratios expressed as ratios of the absolute values of the relative locations of the three ICVs on the three other Aronhold-Kennedy lines, see Figure 17, have never been stated explicitly as:

$$\frac{\dot{\theta}_1}{\dot{\theta}_2} = \frac{d_{P_{24}P_{12}}}{d_{P_{24}P_{12}} + d_{P_{12}P_{14}}}; \tag{33}$$

$$\frac{\dot{\theta}_3}{\dot{\theta}_2} = \frac{d_{P_{13}P_{12}}}{d_{P_{13}P_{12}} + d_{P_{12}P_{23}}}; \tag{34}$$

$$\frac{\dot{\theta}_4}{\dot{\theta}_3} = \frac{d_{P_{24}P_{23}}}{d_{P_{24}P_{23}} + d_{P_{23}P_{34}}}. \tag{35}$$

Additionally, Equations (25) and (28) are angular velocity ratios in terms of distance and configuration. These results yield a measure of all six angular velocity ratios with the six additional Equations (24)-(29).

3.5. Example: Velocity Ratio

In this section we shall illustrate the validity of our generalised Freudenstein theorem ratios of relative distances between ICVs on the four Aronhold-Kennedy lines and explicitly computed angular velocity ratios. For this example the linkage and configuration illustrated in Figure 17 is used with the lengths (generic units) and angles (degrees) listed in Table 9.

Using these parameters, the four Aronhold-Kennedy lines, and the extended Freudenstein theorem yields:

$$\left.\begin{aligned}
\frac{d_{P_{13}P_{14}}}{d_{P_{13}P_{14}} + d_{P_{14}P_{34}}} &= 1.0657 = \frac{\dot{\theta}_4}{\dot{\theta}_1}; \\
\frac{d_{P_{24}P_{12}}}{d_{P_{24}P_{12}} + d_{P_{14}P_{12}}} &= -3.9492 = \frac{\dot{\theta}_1}{\dot{\theta}_2}; \\
\frac{d_{P_{13}P_{12}}}{d_{P_{13}P_{12}} + d_{P_{12}P_{23}}} &= -1.2595 = \frac{\dot{\theta}_3}{\dot{\theta}_2}; \\
\frac{d_{P_{24}P_{23}}}{d_{P_{24}P_{23}} + d_{P_{23}P_{34}}} &= 3.3419 = \frac{\dot{\theta}_4}{\dot{\theta}_3}.
\end{aligned}\right\} \tag{36}$$

The negative or positive sign multiplying the ratio indicates whether or not the two angular velocities have the same sense. Compared to the angular velocities obtained with the six angular velocity ratios computed with suitable variants of Equation (24), we obtain four identical ratios in addition to two, which are not possible to compute directly as ratios of ICVs:

$$\left.\begin{aligned}
\frac{\dot{\theta}_4}{\dot{\theta}_1} &= 1.0657; \quad \frac{\dot{\theta}_3}{\dot{\theta}_2} = -1.2595; \\
\frac{\dot{\theta}_1}{\dot{\theta}_2} &= -3.9492; \quad \frac{\dot{\theta}_4}{\dot{\theta}_2} = -4.2085; \\
\frac{\dot{\theta}_3}{\dot{\theta}_1} &= 0.3189; \quad \frac{\dot{\theta}_4}{\dot{\theta}_3} = 3.3419.
\end{aligned}\right\} \tag{37}$$

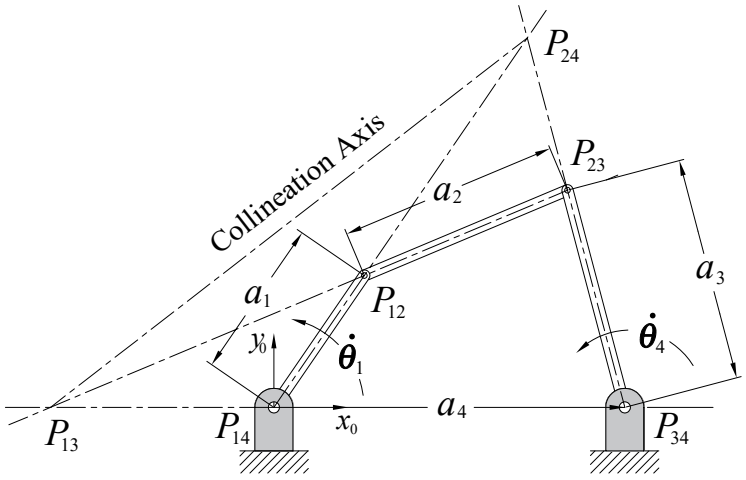

Fig. 18. The collineation axis.

3.6. Corollary to Freudenstein's Theorem 2

Freudenstein's second theorem [31, 32] states that *at an extreme value of the velocity ratio in a four-bar linkage, the collineation axis is perpendicular to the longitudinal centreline of the coupler*. The collineation axis is defined to be the line containing the two secondary ICVs, P_{13} and P_{24}, see Figure 18.

We propose the following corollary to Freudenstein's Theorem 2: *the velocity ratio becomes unity in a four-bar linkage when the collineation axis and the coupler centre line are parallel to the x_0-axis*. Figures 19a and 19b illustrate instances of Theorem 2, and it's corollary being true. To prove the corollary it suffices to consider a drag-link (double crank) planar 4R with a_4 being the shortest link. In this Grasshof inversion case, the coupler can rotate freely through 2π radians and the coupler must therefore align with the x_0-axis direction in two configurations in each of two assembly modes. Figure 19b illustrates one such configuration placing P_{13} at infinity. If the link lengths can form a convex quadrangle in one of these configurations, in the other, of the same assembly mode, it forms a complex quadrangle where a_1 and a_3 cross each other. A configuration illustrating a complex quadrangle appears in Figure 20b.

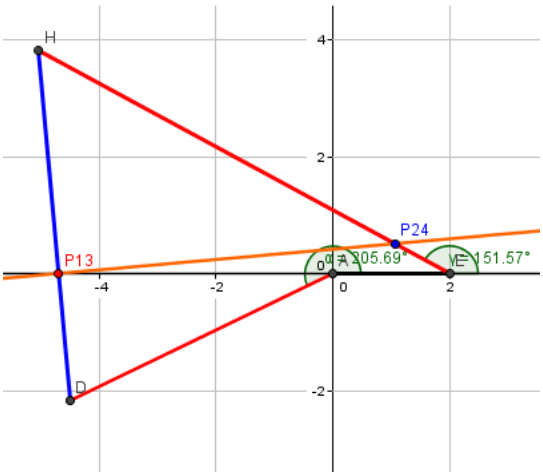

(a) The collineation axis is perpendicular to the coupler.

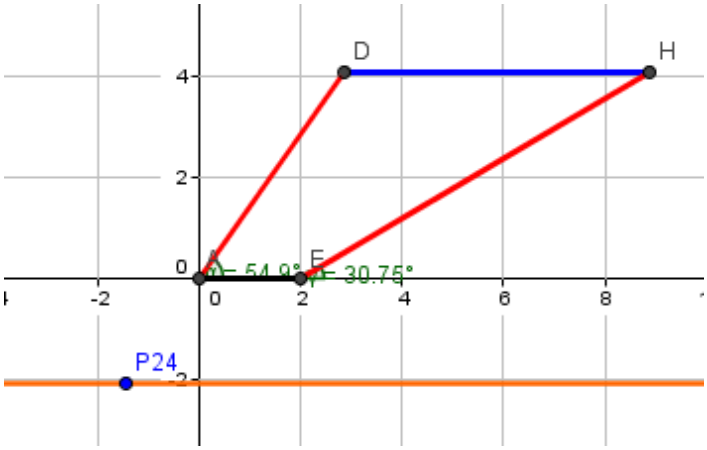

(b) The collineation axis and coupler are parallel to the x_0-axis, the linkage is a convex quadrangle.

Fig. 19. Assembly Mode 1 collineation axes.

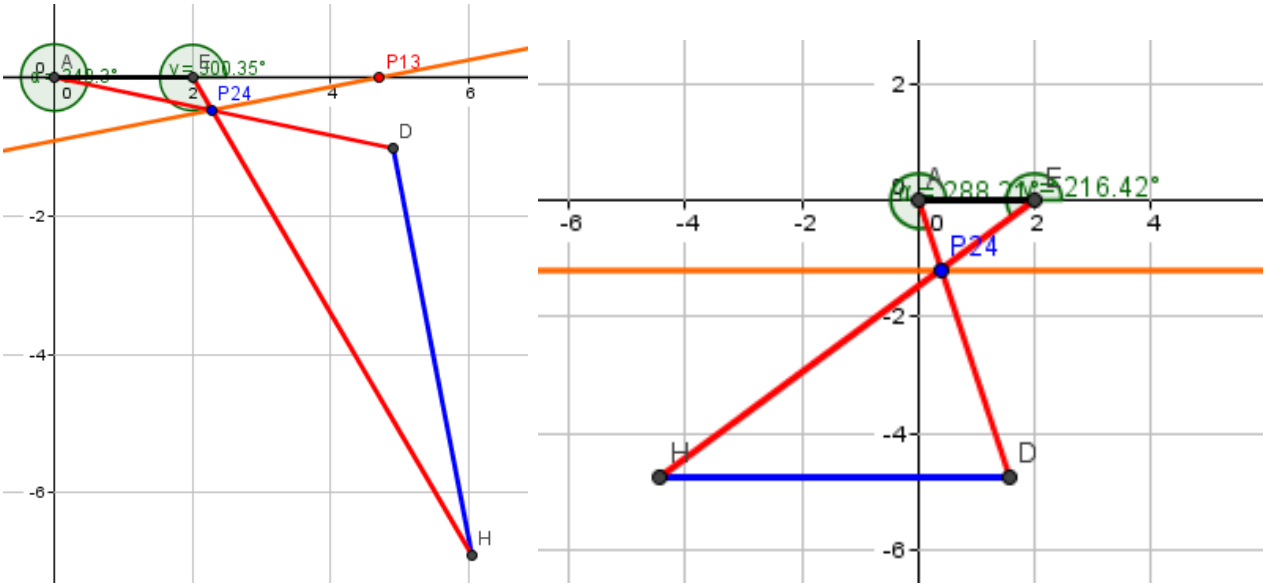

(a) The collineation axis is again perpendicular to the coupler.

(b) The collineation axis and coupler are again parallel to the x_0-axis, the linkage is a complex quadrangle.

Fig. 20. Assembly Mode 2 collineation axes.

To identify the locations of the positions of P_{13} where it is instantaneously at rest and changing directions on the x_0-axis, we require the longitudinal centreline equation of the coupler to determine its point of intersection with the x_0-axis. Using the point-slope form of the planar line equation it is a simple matter to compute the location of P_{13} given any value v_1 and the corresponding value of v_4 revealing

$$P_{13} = \frac{a_1(a_3 v_1^2 v_4 + (a_4 - a_3) v_1 v_4^2 + (a_3 + a_4) v_1 - a_3 v_4)}{a_1 v_1 v_4^2 - a_3 v_1^2 v_4 + a_1 v_1 - a_3 v_1}. \tag{38}$$

We now solve Equation (2) for v_4 and substitute the results back into Equation (38) yielding two equations for P_{13} in terms of v_1, one corresponding to each assembly mode. Next, we identify the critical values of v_1 revealing the extreme locations of P_{13}. These critical values are obtained by setting the derivative of the equation with respect to v_1 equal to 0 and computing $v_{1_{\text{crit}}}$ as:

$$\frac{dP_{13}}{dv_1} = 0. \tag{39}$$

Equation (39) is of degree 6 in v_1 meaning that there are six values for $v_{1_{\text{crit}}}$. It turns out that two of these critical angle parameters are those for which the collineation axis is perpendicular to the centreline of the coupler while four are two pairs of complex conjugates, which do not place P_{13} at infinity, given the way Equation (38) is derived.

To identify the joint angle parameters that locate P_{13} where the coupler centreline, the collineation axis, and the x_0-axis all intersect in a point at infinity we must adopt a different strategy: in this case P_{13} has a non-zero y_0-coordinate. Both configurations where the collineation axis, coupler, and x_0-axis are all parallel impose two useful conditions on the joint angle parameters.

The first condition requires that

$$\theta_1 + \theta_2 \quad = \quad 2\pi. \tag{40}$$

Converting this condition to its algebraic form leads to the very convenient result

$$\textbf{Condition 1}: \quad v_1 + v_2 \;=\; 0. \tag{41}$$

We can use Equation (3), the v_1-v_2 IO equation, to identify two values of $v_{1_{\text{crit}}}$. To do this, we solve Equation (3) for v_2:

$$v_2 \;=\; \frac{-4a_2a_4v_1 \pm \sqrt{\left((A_1B_1v_1^2+C_2D_2)(A_2B_1v_1^2+A_1C_1)\right)}}{A_1B_1v_1^2+C_1D_2}. \tag{42}$$

Substitute each result into Equation (41) in order to obtain two quadratic equations in v_1, one pair for each assembly mode.

As previously mentioned, for the drag-link mechanism there is one configuration where the coupler, collineation axis, and the x_0-axis are all parallel that requires links a_1 and a_3 to cross each other. Figure 21 illustrates a drag-link mechanism in both the upper convex and lower complex quadrangle configurations. In order for Condition 1 to be true in both configurations, we must measure θ_2 with respect to the negative a_2 direction when links a_1 and a_3 cross.

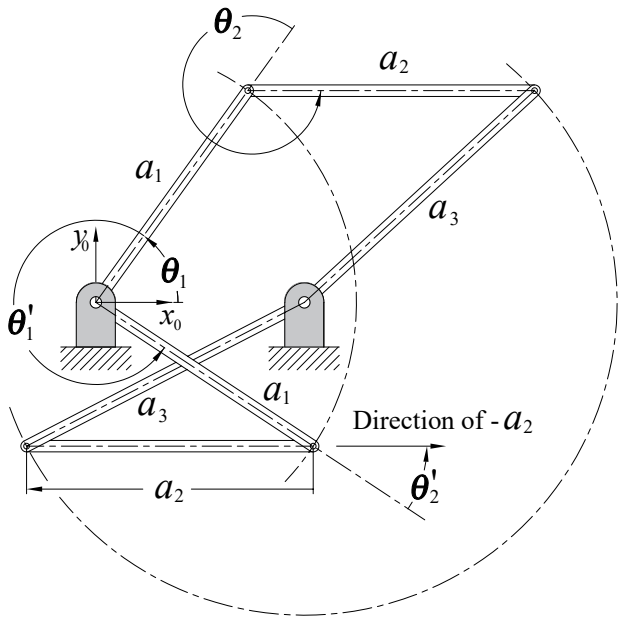

Fig. 21. The collineation axis and coupler are parallel to the x_0-axis in each of two assembly modes.

The second condition requires the coupler-connected ends of links a_1 and a_3 to have the same y_0-coordinate values. This means that

$$a_1 \sin\theta_1 - a_3 \sin\theta_4 \;=\; 0 \tag{43}$$

which becomes

$$\textbf{Condition 2}: \quad a_1\frac{2v_1}{1+v_1^2} - a_3\frac{2v_4}{1+v_4^2} \;=\; 0 \tag{44}$$

using the tangent half-angle equivalents. Solving Equation (44) for v_4 yields

$$v_4 \;=\; \frac{a_3(1+v_1^2) \pm \sqrt{a_3^2(v_1^4+2v_1^2+1) - 4a_1v_1^2}}{2a_1v_1}. \tag{45}$$

Having first obtained v_1 from Equations (41) and (42), it is a simple matter to determine the corresponding v_4 with Equation (45).

These two conditions, unique to the two configurations where the collineation and x_0-axes along with the coupler are all parallel, can be used to identify the required values for θ_1 and θ_4, and are summarised in Table 10.

Table 10. Conditions for coupler being parallel to x_0-axis.

Condition 1	$v_1 + v_2 = 0$
Condition 2	$v_4 = \frac{a_3(1+v_1^2) \pm \sqrt{a_3^2(v_1^4+2v_1^2+1) - 4a_1v_1^2}}{2a_1v_1}$

Table 11. Results for Extrema Example.

$\theta_{1_{\text{crit}_1}}$	-154.3136°	P_{13_1}	-4.6987	$\left(\dot{\theta}_4/\dot{\theta}_1\right)_1$	0.7014
$\theta_{1_{\text{crit}_2}}$	-11.7026°	P_{13_2}	4.6987	$\left(\dot{\theta}_4/\dot{\theta}_1\right)_2$	1.7411
$\theta_{1_{\text{crit}_3}}$	54.9004°	P_{13_3}	∞	$\left(\dot{\theta}_4/\dot{\theta}_1\right)_3$	1
$\theta_{1_{\text{crit}_4}}$	-71.7900°	P_{13_4}	∞	$\left(\dot{\theta}_4/\dot{\theta}_1\right)_4$	1

We will now consider an example of locating the extreme values of P_{13} for a drag-link where P_{13} has four extreme values, two finite and two at infinity. However, the two at infinity do not, in general, represent extreme velocity ratios, rather they represent configurations where the input and output links instantaneously possess the same angular velocity magnitudes.

3.7. Example: Extreme Locations of P_{13}

Using the link lengths already listed in Table 9 and applying the critical values for v_1 in Equation (39) we obtain the extreme finite values for P_{13}. Then to identify the critical values for v_1 that place P_{13} at infinity where the coupler as well as the collineation and x_0-axes intersect, we use Equations (41) and (42). It is a simple matter to compute the corresponding joint angles. The results are listed in Table 11. These are the same results as illustrated in Figures 19a-20b.

3.8. Acceleration Level Kinematics

The acceleration level IO equations express the angular acceleration parameter generated by joint angle parameter v_j in terms of v_i. The $\ddot{v}_1$-$\ddot{v}_4$ IO equation expresses $\ddot{v}_4$ in terms of $\ddot{v}_1$ at any instant in time as a function of the configuration at that time. That is, if a set of numerical values for four constant link lengths a_1-a_4 are given in a feasible state of numerical values for v_1, v_4, $\dot{v}_1$, $\dot{v}_4$, and $\ddot{v}_1$, then $\ddot{v}_4$ is determined. This in turn means that if the mass centres and distributions are known, the extreme values for $\ddot{v}_1$, and $\ddot{v}_4$ can be used to identify the extreme values of the bearing reaction forces generated by the motion.

According to Freudenstein in [31], the maximum output angular acceleration, assuming constant input angular velocity is computed first for a crank-rocker then drag-link as

$$\ddot{\theta}_{4_{\max}} = \frac{\dot{\theta}_1^2 a_1}{a_2 a_3}(a_1 + a_2) \quad \text{and} \quad \frac{\dot{\theta}_1^2 a_4}{a_2 a_3}(a_2 + a_4). \tag{46}$$

But the configuration conditions he lists in the paper are incorrect, moreover the crank-rocker and drag-link he uses in an example are actually both non-Grashof double-rockers. We have developed a novel method using Equation (47), and is briefly summarised here as an algorithm which yields correct results.

The time derivative of Equation (20) is

$$((Av_4^2 + B)v_1 - 4a_1a_3v_4)\ddot{v}_1 + ((Av_1^2 + C)v_4 - 4a_1a_3v_1)\ddot{v}_4 + (Av_4^2 + B)\dot{v}_1^2 + (Av_1^2 + C)\dot{v}_4^2 + (4Av_1v_4 - 8a_1a_3)\dot{v}_1\dot{v}_4. \tag{47}$$

The angular acceleration parameters, $\ddot{v}_i$, are related to the angular accelerations, $\ddot{\theta}_i$, as

$$\ddot{v}_i \;=\; \frac{1}{2}(\ddot{\theta}_i + \dot{\theta}_i{}^2 v_i)(1 + v_i^2), \tag{48}$$

and

$$\ddot{\theta}_i \;=\; \frac{2\ddot{v}_i}{(1 + v_i^2)} - \dot{\theta}_i^2 v_i. \tag{49}$$

The five other angular acceleration parameter equations are

$$\begin{aligned}((A_1B_1v_2^2 + A_2B_2)v_1 + 4a_2a_4v_2)\ddot{v}_1 + ((A_1B_1v_1^2 + C_1D_2)v_2 + 4a_2a_4v_1)\ddot{v}_2 + \\ (A_1B_1v_2^2 + A_2B_2)\dot{v}_1^2 + (A_1B_1v_1^2 + C_1D_2)\dot{v}_2^2 + (4A_1B_1v_1v_2 + 8a_2a_4)\dot{v}_1\dot{v}_2,\end{aligned} \tag{50}$$

$$(A_2B_1v_3^2 + A_1B_2)v_1\ddot{v}_1 + (A_2B_1v_1^2 + C_1D_1)v_3\ddot{v}_3 + (A_2B_1v_3^2 + A_1B_2)\dot{v}_1^2 + (A_2B_1v_1^2 + C_1D_1)\dot{v}_3^2 + 4A_2B_1v_1v_3\dot{v}_1\dot{v}_3, \tag{51}$$

$$\begin{aligned}((B_1C_1v_3^2 + A_1D_2)v_2 - 4a_1a_3v_3)\ddot{v}_2 + ((B_1C_1v_2^2 + A_2D_1)v_3 - 4a_1a_3v_2)\ddot{v}_3 + \\ (B_1C_1v_3^2 + A_2D_1)\dot{v}_2^2 + (B_1C_1v_2^2 + A_2D_1)\dot{v}_3^2 + (4B_1C_1v_2v_3 - 8a_1a_3)\dot{v}_2\dot{v}_3,\end{aligned} \tag{52}$$

$$(A_1C_1v_4^2 + B_1D_2)v_2\ddot{v}_2 + (A_1C_1v_2^2 + A_2C_2)v_4\ddot{v}_4 + (A_1C_1v_4^2 + B_1D_2)\dot{v}_2^2 + (A_1C_1v_2^2 + A_2C_2)\dot{v}_4^2 + 4A_1C_1v_2v_4\dot{v}_2\dot{v}_4, \tag{53}$$

$$\begin{aligned}((A_2C_1v_4^2 + B_1D_1)v_3 + 4a_2a_4v_4)\ddot{v}_3 + ((A_2C_1v_3^2 + A_1C_2)v_4 + 4a_2a_4v_3)\ddot{v}_4 + \\ (A_2C_1v_4^2 + B_1D_1)\dot{v}_3^2 + (A_2C_1v_3^2 + A_1C_2)\dot{v}_4^2 + (4A_2C_1v_3v_4 + 8a_2a_4)\dot{v}_3\dot{v}_4.\end{aligned} \tag{54}$$

3.9. Algorithm for Computing Maximum Angular Accelerations and Critical Input Angles

The substitution techniques used to compute the critical values of $\theta_{1_{\text{crit}}}$ and corresponding extreme values for $\ddot{\theta}_{4_{\min/\max}}$ require transforming the algebraic angular acceleration parameter $\ddot{v}_i$-$\ddot{v}_j$ equations to their corresponding trigonometric angular acceleration $\ddot{\theta}_i$-$\ddot{\theta}_j$ equations. The condition that the input angular velocity is constant must be used, however, this is not unreasonable in practise. Regardless, the resulting equations contain large numbers of terms and are very cumbersome to manipulate accurately with pen and paper: symbolic computer algebra software such as Maple, Matlab, or MathCAD should be used.

The distinct advantage of using Equations (47)-(54) is that the maximum and minimum angular accelerations, and the configurations they occur in, can always be computed. To the best of the author's collective knowledge, this has not been possible before. The algorithm presented here, and the results in [35], are entirely new, and revealed here for the first time! The approach is stated algorithmically next. These algorithm

steps are not unique, there are many subtle variations to the steps and you are encouraged to experiment with your own.

Algorithm

1. Convert the two variable angle parameters v_1 and v_4 to angles as $v_i = \tan\theta_i/2$ and solve for θ_4, there will be two solutions.

2. Substitute each expression for θ_4 into the $\dot{\theta}_1$-$\dot{\theta}_4$ equation and solve the resulting for $\dot{\theta}_4$.

3. Substitute the expressions for θ_4 and $\dot{\theta}_4$ into the $\dot{v}_1$-$\dot{v}_4$ equation after you have substituted $v_i = \tan(\theta_i/2)$ and Equations (22) and (48).

4. Solve the resulting equation for $\ddot{\theta}_4$ and substitute the specified value for $\dot{\theta}_1$. You now have an equation for $\ddot{\theta}_4$ in terms of θ_1 as the only variable.

5. Because $\dot{\theta}_1$ is constant means that $\ddot{\theta}_1 = 0$, so the equation determined in Step 4 is

$$\ddot{\theta}_4 \quad = \quad f(\theta_1)$$

6. To determine the critical values of the input angle $\theta_{1_{\text{crit}}}$ where the output angular acceleration is an extreme value, either the greatest positive or negative value, determine the derivative of $\ddot{\theta}_4 = f(\theta_1)$ with respect to θ_1.

7. The extreme values of $\ddot{\theta}_4$ occur at the values of $\theta_{1_{\text{crit}}}$ that cause the following equation to be satisfied:

$$\frac{d\left(\ddot{\theta}_4 = f(\theta_1)\right)}{d\theta_1} \quad = 0.$$

8. If you obtain the solution using Maple, you will be faced with four real values for $\theta_{1_{\text{crit}}}$, and 18 complex solutions.

9. Determine the corresponding values for $\ddot{\theta}_{4_{\text{max/min}}}$ and you should see that only two are distinct, one corresponding to a pair of values for $\theta_{1_{\text{crit}}}$, the other pair corresponding to the other extreme value of $\ddot{\theta}_4$.

3.10. Example: Extreme Output Angular Acceleration

We now continue the example whose results are listed in Table 11 and identify the maximum value for the output angular acceleration, $\ddot{\theta}_4$. Without loss of generality we assign a constant angular velocity for the input link of $\dot{\theta}_1 = 10$ rad/s. While this means $\ddot{\theta}_1 = 0$, it also means that $\dot{v}_1 \neq 0$, as is required by the angular velocity and angle parameter dependency of Equation (48). Since the linkage considered is a drag-link we use the second form of Equation (46) and obtain the value of $\ddot{\theta}_4$ The results are listed in Table 12.

Table 12. Maximum $\ddot{\theta}_4$ results.

$\theta_{1_{\text{crit}_1}}$	=	12.3685°	$\theta_{1_{\text{crit}_2}}$	=	-39.4289°
$\dot{\theta}_{4_{\text{crit}_1}}$	=	14.7804 rad/s	$\dot{\theta}_{4_{\text{crit}_2}}$	=	14.3701 rad/s
$\ddot{\theta}_{4_{\text{max}_1}}$	=	96.1559 rad/s^2	$\ddot{\theta}_{4_{\text{max}_2}}$	=	-92.5833 rad/s^2

4. FUNCTION GENERATOR SYNTHESIS

In this section we will solve the exact kinematic synthesis problem for a planar RRRP function generating mechanism. Mechanism synthesis involves determining the link lengths required to generate a particular type of desired motion. Most automated manufacturing and assembly mechanical systems require four-bar mechanisms where the output link moves as a particular function of the input link motion to position a tool to execute a desired task. Since the general planar RRRP algebraic IO equation contains only three design parameters: the three unknown link lengths a_1, a_2, and a_4, assuming the offset directed distance a_4 is perpendicular to the slider direction of reciprocating translation with $v_4 = 1$. If the desired task can be modelled with three precise slider locations that are functions of the input link angle θ_1, or angle parameter $v_1 = \tan(\theta_1/2)$, then we can generate three synthesis equations with $a_{3_i} = f(\theta_{1_i})$, where i is not the complex number $\sqrt{-1}$ but is instead a counting index whose value is 1, 2, or 3 determined by each of the three IO pairs (each pair of input angle and slider location *precision values*). Then, it is a simple matter to solve the three IO equations for the three unknown link lengths a_1, a_2, and a_4. Since the three IO equations are quadratic in the link lengths, there will in general be two solutions. Let's now examine the meaning of these two possible solutions with several examples.

Consider a beer bottle capping system. Full bottles of beer move along a conveyor belt at a constant rate with specific constant distances between the bottles. The device that places the cap on the bottle must move at the same rate as, and parallel to the conveyor, place and crimp a cap on the bottle, then return to a kinematically neutral location to start the process again. This continuous process can be modelled as the bottling operation for a single bottle, but as an infinitely repeating single discrete step: the bottle enters a control volume, moves at a constant rate along a rigidly defined path, maintained by a funneling chute, to a location where the capping tool held by the output link of an RRRP mechanism places and crimps the cap; the next bottle enters the control volume as the RRRP linkage returns to crimp a cap it.

4.1. Planar RRRP Algebraic IO Equation

Consider the planar RRRP linkage illustrated in Figure 22a. The variables are the input joint angle θ_1' and the slider translation distance a_3' while the design parameters are the constant link lengths a_1, a_2, a_4', and the inclination angle of the P-pair, $v_4' = \tan(\theta_4'/2)$. Re-collecting Equation (2) in terms of $v_1' = \tan(\theta_1'/2)$ and a_3' yields

$$\begin{gathered}(v_4'^2+1)v_1'^2a_3'^2+(v_4'^2+1)a_3'^2+2(v_4'-1)(v_4'+1)(a_1-a_4')a_3'-8a_1a_3'v_4'v_1'- \\ 2(v_4'-1)(v_4'+1)(a_1+a_4)v_1'^2a_3'+(a_1+a_2+a_4')(a_1-a_2+a_4')(v'4^2+1)v_1'^2+ \\ (a_1+a_2-a_4')(a_1-a_2-a_4')(v_4'^2+1)=0.\end{gathered} \tag{55}$$

Without loss in generality, the general design constant slider angle θ_4', illustrated in Figure 22a, can always be set to $\pi/2$ with a suitable transformation of the x_0'-y_0' coordinate system, such that the distance a_4' along the x_0'-axis is transformed to the different distance a_4 along the new x_0-axis which is orthogonal to the longitudinal axis of symmetry (the centre-line) of the slider, as illustrated in Figure 22b. In other words,

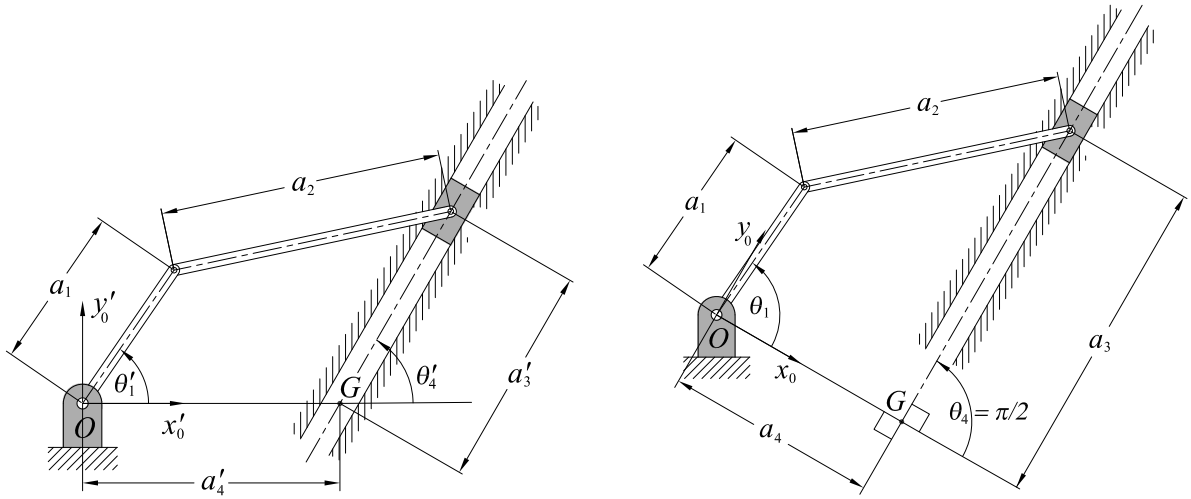

(a) General P-pair orientation.

(b) Orthogonal P-pair orientation.

Fig. 22. Planar RRRP linkage.

by rotating x_0'-y_0' about it's origin to x_0-y_0 so that $\theta_4 = \pi/2$. This will change the length of a_4' to a_4 and the location of point G on the P-pair longitudinal centre-line thereby changing the zero for the slider translation a_3. Regardless, any RRRP linkage can be so represented [27, 30]. Making the substitution

$$\theta_4 \;=\; \frac{\pi}{2} \quad \Rightarrow \quad v_4^{'} \;=\; \tan\left(\frac{\theta_4}{2}\right) \;=\; 1$$

in Equation (55) makes several terms vanish revealing a more compact and elegant, but still completely general, RRRP algebraic IO equation:

$$v_1^2 a_3^2 + A v_1^2 + a_3^2 - 4 a_1 v_1 a_3 + B \;=\; 0, \tag{56}$$

where

$$\begin{aligned} A \;&=\; A_1 A_2 \;=\; (a_1 + a_2 + a_4)(a_1 - a_2 + a_4), \\ B \;&=\; B_1 B_2 \;=\; (a_1 + a_2 - a_4)(a_1 - a_2 - a_4), \\ v_1 \;&=\; \tan\left(\frac{\theta_1}{2}\right); \quad v_4 \;=\; \tan\left(\frac{\theta_4}{2}\right) \;=\; \tan\left(\frac{\pi/2}{2}\right) \;=\; 1. \end{aligned}$$

4.2. Example 4.1: Negative Link Lengths

Before computing possible link lengths the junior engineer in charge of determining the function governing the motions makes the design decision to mount the P-pair sliding direction to be parallel to the conveyor direction and that the shaft of RRRP actuator motor is perpendicular to the conveyor and slider travel directions, and we assign the x_0-axis to be the common normal between the motor shaft axis and the P-pair longitudinal centre line. Suppose that the function correlating the slider location to the shaft angle is

$$a_3 \;=\; -\frac{9}{4}\sin(\theta_1) - 3. \tag{57}$$

Suppose further that the precision input angles and output values of a_3 that exactly satisfy the function specified by Equation (57) are empirically determined by the junior engineer, who measures the IO pairs

i^{th} pair	Input angle (deg) θ_{1_i}	Slider location a_{3_i}
$i=1$	5°	-3.196100421 cm
$i=2$	40°	-4.446272122 cm
$i=3$	85°	-5.241438071 cm

Table 13. Precision I0 pairs for uniform input angle spacing.

with a very precise laser theodolite that is set up on one side of the conveyor, to be those listed in Table 13 where the angles are specified in degrees and the lengths in centimetres. Notice that the function requires that θ_1 and a_3 increase in opposite directions: as θ_1 increases a_3 decreases. Populating Equation (56) with the three IO pairs yields the following three equations:

$$\begin{aligned}
10.23453064 + 0.5581790323a_1 + 0.1906277937e^{-2}(a_1-a_2+a_4)(a_1+a_2+a_4)+(a_1-a_2-a_4)(a_1+a_2-a_4) &= 0;\\
22.38826533 + 6.473242823a_1 + 0.1324743315(a_1-a_2+a_4)(a_1+a_2+a_4)+(a_1-a_2-a_4)(a_1+a_2-a_4) &= 0;\\
50.54045520 + 19.21157241a_1 + 0.8396628208(a_1-a_2+a_4)(a_1+a_2+a_4)+(a_1-a_2-a_4)(a_1+a_2-a_4) &= 0.
\end{aligned}$$

Solving the three equations simultaneously for the three unknown link lengths a_1, a_2, and a_4 gives the two solutions listed in Table 14

Solution	a_1	a_2	a_4
1	-1.952184536 cm	3.321470078 cm	-0.5751750055 cm
2	-1.952184536 cm	-3.321470078 cm	-0.5751750055 cm

Table 14. The two solutions to the exact synthesis problem.

The junior engineer is puzzled: what does a *negative length* mean? Euclidean geometry very explicitly states that distances are always greater than or equal to zero, but never less than zero [36]. The explanation lies in the fact that the link lengths are really directed distances. Consider a unit position vector locating the point $(x,y)=(1,1)$. Multiplying the vector by the scalar -1 simply rotates the vector direction by $\pi = 180^\circ$ making it locate the point $(x,y)=(-1,-1)$. Both vectors are oriented at 45° relative to the positive x-axis and their magnitudes are both $\sqrt{2}$, but they point in opposite directions.

The directed distance -1.952184536 cm represents the input link. In the second precision configuration of the mechanism a_1 is oriented at 40° relative to the positive x_0-axis indicated in Figure 22, but points in the opposite direction to the centre line of a_1, this is graphically illustrated in Figure 23. Since a_4 always points along the x_0-axis, a negative value for this distance simply places the slider centre line along the negative x_0-axis.

The sign of the coupler directed distance, a_2, is of no consequence in the shape coefficients of the RRRP algebraic IO equation. Only the coefficients A and B in Equation (56) contain the coupler length a_2. Expanding these two coefficients leads to

$$A = A_1A_2 = (a_1+a_2+a_4)(a_1-a_2+a_4) = a_1^2+2a_1a_4-a_2^2+a_4^2; \tag{58}$$

$$B = B_1B_2 = (a_1+a_2-a_4)(a_1-a_2-a_4) = a_1^2-2a_1a_4-a_2^2+a_4^2. \tag{59}$$

The shape of the algebraic IO equation of every planar RRRP function generating mechanism is affected by the number $-a_2^2$, which is always a negative number regardless of the sign of the numerical value of a_2.

The complete mobility classification of the input link requires both positive and negative values of the coupler directed length $\pm a_2$. Since the coupler correlates the rotation of the input link to the translation

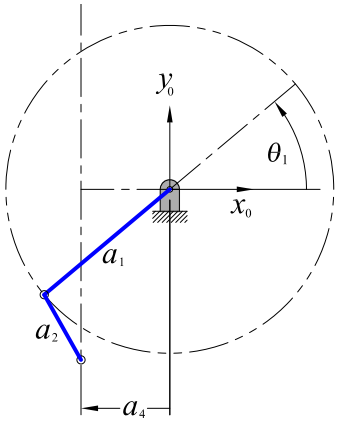

Fig. 23. Negative link length meaning for a_1 and a_4.

(linear, or curvilinear) of the slider then directed distance $+a_2$ points from the distal R-pair centre of the input link to the R-pair connecting the coupler to the slider. The directed distance $-a_2$ simply points in the opposite direction: from the R-pair centre connecting the coupler to the slider to the distal R-pair centre of the input link. Therefore, relative to the non-moving coordinate system x_0-y_0, the direction of the length a_2 has no effect on the generated function, but it's sign affects the input link mobility classification.

4.3. Uniform and Chebyshev Distribution of Precision Configurations

For many applications exact synthesis is sufficient. In fact, before computers that could perform the numerical optimisation of large IO sets existed, three precision configuration synthesis was essentially all that was available. You will note that in the preceding exact synthesis problem that the specified input angles were uniformly distributed over the desired input angle range between 5°-85°. In the 1840s P.L. Chebyshev reasoned that the structural error function of the generated output of the linkage subtracted from the specified function output could be analysed to locate inflection points on the associated curve where the tangent is horizontal [37]. At these locations the error of the output is insensitive to changes in input, so these should be the values for the IO precision configurations. For a planar RRRP linkage the three precision configurations are located according to the following equation using the Chebyshev distribution function:

$$\theta_{1_i} = a + h\cos\left(\frac{(2i-1)\pi}{6}\right), \quad i \in \{1,2,3\}, \tag{60}$$

where

$$a = \frac{1}{2}(\theta_{1_{\text{initial}}} + \theta_{1_{\text{end}}}) \tag{61}$$

and

$$h = \frac{1}{2}(\theta_{1_{\text{end}}} - \theta_{1_{\text{initial}}}) \tag{62}$$

so that a_3 satisfies the function at the three values of θ_{1_i}. Again, the letter i is not the imaginary number $\sqrt{-1}$, rather it is a counting index whose value is 1, 2, or 3.

4.4. Example 4.2

We will consider the exact synthesis problem with Chebyshev spacing for approximating the function in Equation (57). Let us compute the Chebyshev distribution of the IO pairs using Equation (60) in an effort

reduce the structural error to its minimum value for three IO precision configurations. Note that the angular ranges a and h must be specified in radians, and the value computed for θ_{1_i} will also be given in radians. Note further that these IO pairs will be ordered from large to small because of the way the ratio is specified.

The Chebyshev distribution for input angles and output slider locations is listed in Table 15. The three

i^{th} pair	Input angle θ_{1_i} (rad)	Slider location a_{3_i}
$i=1$	$(1/4)\pi+(1/9)\pi\sqrt{3}$	-5.213326005 cm
$i=2$	$(1/4)\pi$	-4.590990258 cm
$i=3$	$(1/4)\pi-(1/9)\pi\sqrt{3}$	-3.404583734 cm

Table 15. Precision IO pairs for Chebyshev spacing.

synthesis equations have the form:

$$\begin{aligned}
46.07293212+17.38696712a_1+0.6951810353(a_1-a_2+a_4)(a_1+a_2+a_4)+(a_1-a_2-a_4)(a_1+a_2-a_4) &= 0;\\
24.69346590+7.606601721a_1+0.1715728754(a_1-a_2+a_4)(a_1+a_2+a_4)+(a_1-a_2-a_4)(a_1+a_2-a_4) &= 0;\\
11.68643221+1.234450898a_1+0.8216741368e^{-2}(a_1-a_2+a_4)(a_1+a_2+a_4)+(a_1-a_2-a_4)(a_1+a_2-a_4) &= 0.
\end{aligned}$$

These three synthesis equations are solved simultaneously for the three unknown link lengths and are listed in Table 16. The three link lengths are somewhat different from those for the uniform distribution listed in Table 14. If a structural error analysis were performed on the both sets of link lengths one would find that the area between specified and generated functions, the structural error, would be smaller for the Chebyshev spacing.

Solution	a_1	a_2	a_4
1	-1.908252574 cm	3.341820771 cm	-0.5372675934 cm
2	-1.908252574 cm	-3.341820771 cm	-0.5372675934 cm

Table 16. The two solutions to the exact synthesis problem with Chebyshev IO spacing.

4.5. Importance of Location and Orientation of Measurement Reference Coordinate Systems

In the previous two examples a junior engineer placed the measurement system reference coordinate system so that the motion of the bottles on the conveyor belt was in a particular direction. Suppose the laser theodolite was positioned and calibrated so that the motion of the conveyor was in the -y direction of the measurement coordinate system. What if the junior engineer was set up on the opposite side of the conveyor when the measurements were made? The conveyor would appear to be moving in the opposite direction: bottles would move parallel to the +y axis of the measurement coordinate system.

4.6. Example 4.3

For the engineer on the other side of the conveyor the function in Equation (57) is multiplied by -1:

$$a_3 = \frac{9}{4}\sin(\theta_1)+3. \tag{63}$$

Meanwhile, the precision IO pairs are now measured to be those listed in Table 17. In this case, a_3 increases as θ_1 increases.

Populating Equation (56) with these three new IO pairs yields the following three equations:

$$\begin{aligned}
10.23453064-0.5581790323a_1+0.1906277937e^{-2}(a_1-a_2+a_4)(a_1+a_2+a_4)+(a_1-a_2-a_4)(a_1+a_2-a_4) &= 0;\\
22.38826533-6.473242823a_1+0.1324743315(a_1-a_2+a_4)(a_1+a_2+a_4)+(a_1-a_2-a_4)(a_1+a_2-a_4) &= 0;\\
50.54045520-19.21157241a_1+0.8396628208(a_1-a_2+a_4)(a_1+a_2+a_4)+(a_1-a_2-a_4)(a_1+a_2-a_4) &= 0.
\end{aligned}$$

i^{th} pair	Input angle θ_{1_i} (deg)	Slider location a_{3_i}
$i = 1$	5°	3.196100421 cm
$i = 2$	40°	4.446272122 cm
$i = 3$	85°	5.241438071 cm

Table 17. Precision I0 pairs for uniform distribution.

This set of three synthesis equations is only different from the first set in that the coefficient for a_1 is now multiplied by -1, but otherwise they are the same. Solving the three equations simultaneously for the three unknown link lengths a_1, a_2, and a_4 gives the two solutions listed in Table 18.

Solution	a_1	a_2	a_4
1	1.952184536 cm	3.321470078 cm	0.5751750055 cm
2	1.952184536 cm	-3.321470078 cm	0.5751750055 cm

Table 18. The two solutions for the exact synthesis problem for generating Equation (63).

In this case the positive value for a_1 of 1.952184536 cm in the second precision configuration of the mechanism a_1 is oriented at 40° relative to the positive x_0-axis indicated in Figure 22 and points in the same direction to the centre line of a_1, this is graphically illustrated in Figure 24. Since a_4 always points along the x_0-axis, a positive value for this distance simply places the slider centre line along the positive x_0-axis.

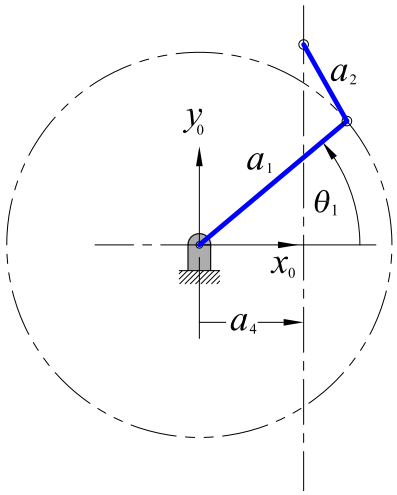

Fig. 24. Conventional link lengths for a_1 and a_4.

The exact function generation synthesis problem will lead to a linkage that exactly generates the desired function between input and output parameters, but only at the three specified precision configurations. For all other reachable intermediate configurations the generated function value will be different from the specified value that satisfies the desired function. This error is known as the *structural error* [8]. If more than three precision configurations are specified the synthesis problem becomes over constrained, but using error optimisation techniques, such as least-squares optimisation, approximate solutions minimising the structural error may be obtained, see [38] for example. The larger the cardinality of the IO pair set, the more the error

is minimised. This has led to the notion of infinite IO data sets obtained using integral vector calculus to obtain an error minimised over the entire IO range [39].

4.7. Summary of Directed Lengths in an RRRP Linkage

In the preceding examples of the results of the kinematic synthesis of planar RRRP function generators we have seen that negative directed link lengths need to be included when generating certain functions defined in certain reference coordinate systems. The input link and coupler can have directed lengths that are greater than or less than zero, but never identically equal to zero. The slider offset distance can be any number along the x_0-axis: negative, zero, or positive:

$$a_1 \begin{cases} > & 0 \\ \neq & 0 \\ < & 0 \end{cases} ; \quad a_2 \begin{cases} > & 0 \\ \neq & 0 \\ < & 0 \end{cases} ; \quad a_4 \begin{cases} > & 0 \\ = & 0 \\ < & 0 \end{cases} .$$

4.8. Branch and Order Defects

Two problems that frequently arise in choosing precision pairs and the input angle range when designing a linkage for function generation and/or motion generation are the *branch defect* and *order defect* problems. The branch defect refers to the situation where a synthesised linkage that meets all mathematical prescribed requirements at each of the precision input angles, but cannot move continuously between all of them without needing to be disassembled from one assembly mode, and reassembled into the other. The order defect is the situation where the linkage can reach all precision poses in the same assembly configuration, but not in the desired order.

As an example of the branch defect, suppose the goal is to generate the following function

$$a_3 \quad = \quad 6\sin(\theta_1) - 1 \tag{64}$$

with an RRRP mechanism over the input angle range of 0°-90°. We choose a uniform distribution of accuracy points over the desired input angle range as

$$v_{1_i} \quad = \quad 0,\ \tan\left(\frac{\pi/4}{2}\right),\ \tan\left(\frac{\pi/2}{2}\right).$$

The values of the output angle parameter, a_3, for each of the specified input angle parameters v_1 are the same as for the previous example

$$\begin{aligned} a_{3_i} \quad &= \quad 6\sin\left(2\tan^{-1}(v_{1_i})\right) - 1 \\ &= \quad -1,\ 3.242640688,\ 5. \end{aligned}$$

We obtain three equations by substituting the IO pairs of each v_{1_i}, a_{3_i} into Equation (56). Solving the three equations for a_1, a_2, and a_4 in Maple yields two distinct solutions where

$$\begin{aligned} &a_1 = 1.500000000, \quad a_2 = 4.609772229, \quad\ a_4 = -3.000000000, \text{ and} \\ &a_1 = 1.500000000, \quad a_2 = -4.609772229, \quad a_4 = -3.000000000. \end{aligned}$$

We select the first solution.

We can draw the linkage using the selected synthesised link lengths revealing the three poses illustrated in Figure 25a. However, we need to compare a plot of the desired function, where the input angle has been converted to $v_1 = \tan(\theta_1/2)$, to the generated IO curve both in the v_1-a_3 plane. The desired function, over a suitably large range for v_1, and the IO curve generated by the selected synthesised linkage is illustrated in

Figure 25b. Note that we can see the structural error; that is the area between the curve of the function and the IO curve in the desired input angle parameter range, i.e. the difference between the specified IO values and the generated IO values over the continuous specified IO range. We observe the first prescribed value for v_1 and corresponding function value for a_3, the blue diamond with coordinates $(0,-1)$ in Figure 25b, lies exactly on the lower assembly mode, or branch. The following two input angle parameter and corresponding specified values for a_3 lie exactly in the upper assembly mode of the selected synthesised linkage. The mechanism cannot generate the function continuously over the desired input angle range without being taken apart and reassembled. This is precisely the branch defect problem. The designer must rethink the precision pose range to attempt to resolve the branch defect.

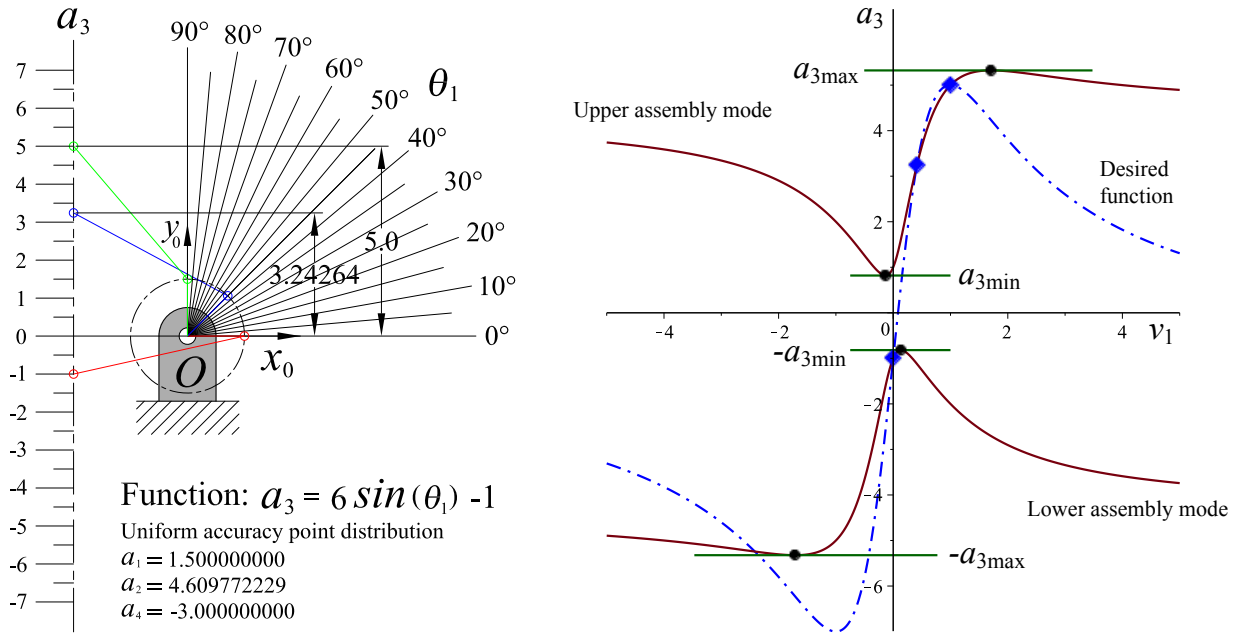

(a) Precision poses for $a_3 = 6\sin(\theta_1) - 1$.

(b) Function and generated IO curve.

Fig. 25. Illustration of branch defect.

5. MULTIPLE POINTS AND ALGEBRAIC CURVES

An *algebraic curve* can be thought of as the path generated by the motion of a point. The curve is algebraic if the path the point traces can be mathematically represented by a polynomial equation in two variables where the coefficients are rational numbers. Planar curves of at least degree three can have multiple distinct branches and locations where the curve intersects itself. Similar statements apply to the algebraic IO curve: since they are degree four they can have multiple closed branches and self-intersect.

5.1. Assembly Modes and Working Modes

If the IO curve has two distinct branches then in order for the linkage to cover points in both branches it must be taken apart and reassembled in a different way. These two distinct linkage configurations, one for each branch of the curve, are called *assembly modes*, and an example of an IO curve with two distinct branches is illustrated in Figure 26a.

Working modes are subtly different. Consider the rocker-slider illustrated in Figure 26b. When the input angle reaches minimum or maximum values the mechanism instantaneously stops moving as the coupler

becomes horizontal. Clearly, care must be taken in designing an actuation system for such linkages as the angular velocity of the motor drive shaft must decelerate, stop, and accelerate in the opposite sense in order to start the linkage moving again. In these configurations the mechanism is said to be *locked* because the coupler force line of action is perpendicular to the slider travel direction. The vertical component of force the coupler can transfer from the input link is zero, and even an infinite amount of torque supplied by the actuator at the base of the input link cannot make the slider move. A torsional spring in the R-pair connecting the coupler to the slider, or some other form of force capacitance, must be designed into the joint to make the slider move again, thereby breaking the lock.

Assuming the locking problem has been resolved, then moving away from these minimum or maximum input configurations the coupler can, in the absence of any compelling forces, arbitrarily continue to move with a_3 either increasing, or decreasing. In Figure 26a the two assembly modes each have two working modes. The two working modes in each assembly mode are separated by the minimum and maximum input angle parameters which occur at the two vertical tangent points on each IO curve branch and represent $v_{1_{\min}}$ and $v_{1_{\max}}$ in the v_1-a_3 plane. At all other points on the IO curve a vertical line intersects it in an upper value for a_3 and a lower value. These are the working modes, and the branching points between each mode occur at $v_{1_{\min}}$ and $v_{1_{\max}}$.

In one working mode the slider can reach it's maximum value, labelled $a_{3_{\max-\mathrm{WM1}}}$ in Figure 26b, when the input link and coupler, a_1 and a_2, align. Whereas in the other working mode a_3 can't reach it's maximum value, the corresponding position is labelled and $a_{3_{\mathrm{WM2}}}$ in Figure 26b. Note that in general in the plot of the algebraic IO curve of the linkage the slider position $a_{3_{\mathrm{WM2}}}$ is always vertically opposed to $a_{3_{\max-\mathrm{WM1}}}$. This phenomenon can be explained by conceptually removing the R-pair connection between the coupler and slider to create a three link open kinematic chain. Now, at every input angle reachable by the closed RRRP linkage in a particular assembly mode the distal end of the coupler, that would normally be pin-connected to the slider, is free to move on a circle centred at the R-pair attachment to the input link. That circle, for all input angles between $\theta_{1_{\min}}$ and $\theta_{1_{\max}}$, or tangent half-angle parameters $v_{1_{\min}}$ and $v_{1_{\max}}$ in the plot of the IO curve, intersects the centre line of the slider in two points, represented by the vertically opposed points on the algebraic IO curve in the v_1-a_3 plane. Once the coupler has started to move either upward or downward in the slider it must continue on that path until the next input angle extreme is reached. Each of these possible slider directions are called working modes.

Assembly and working modes for specific linkages are easily identified by examining a plot of the algebraic IO curve in the v_1-a_3 plane. Assembly modes correspond to distinct branches of the IO curve. Working modes are similarly easily identified: if a vertical line parallel to the a_3-axis intersects a distinct branch of the IO curve in two points then there are two working modes in that assembly mode. Hence, the rocker-slider IO curve illustrated in Figure 26a has two assembly modes, and each one has two working modes.

All planar RRRP linkages can have multiple assembly and working modes and, it turns out, that certain input link angular displacement limits dictate the numbers. For example rocker-sliders that are non-folding (in a mechanism where the link lengths allow $v_1 = 0$ or π, while at the same time $a_3 = 0$, are said to fold with the input link and coupler both laying on the x_0-axis) have two assembly modes each possessing two working modes, meaning that there are maximum and minimum input joint angles where the coupler becomes horizontal in the x_0-y_0 plane. Folding rocker-sliders have two assembly modes, each possessing two working modes, which intersect in a common point at the origin, called a *double point*. Two special subsets of rocker-slider are the so called π- and 0-rocker-sliders. All non-folding π-rocker-sliders rock in the range -$\theta_{1_{\min}}$ to $\theta_{1_{\min}}$ crossing the negative x_0-axis through π. Whereas input links that are 0-rockers rock in the range -$\theta_{1_{\max}}$ to $\theta_{1_{\max}}$ crossing the positive x_0-axis through 0. All non folding π- and 0-rocker-sliders each have but one assembly mode that has two working modes. Finally, all non-folding crank-sliders have two distinct assembly modes each having only one working mode and therefore no limits on the crank rotation

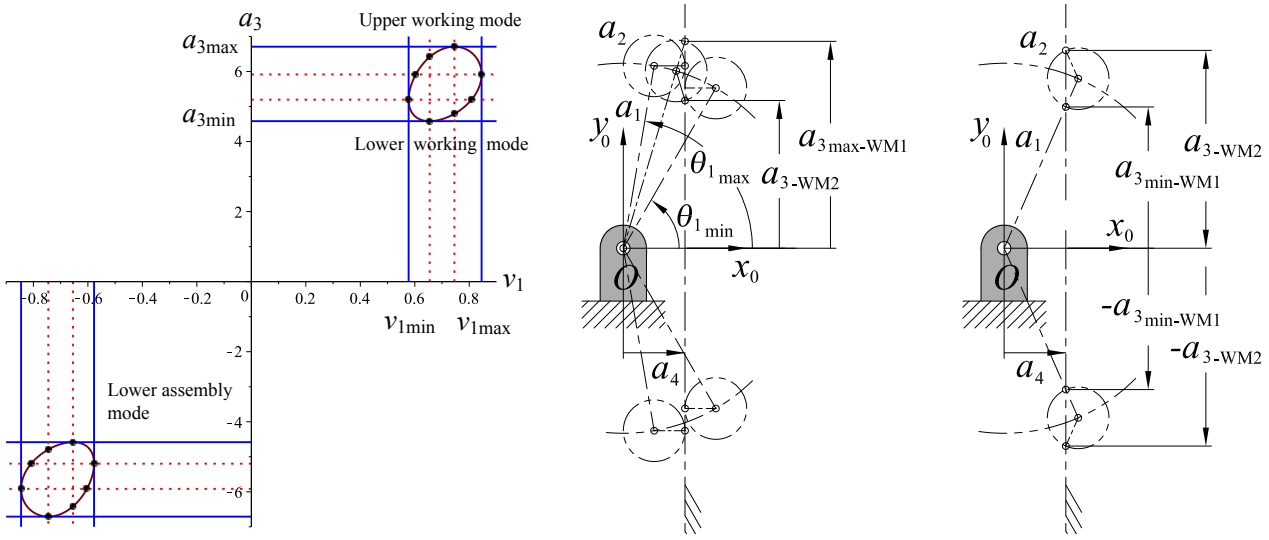

(a) Rocker: $a_1 = 6$, $a_2 = 1$, $a_4 = 2$.

(b) The two assembly and working modes.

Fig. 26. Assembly and working modes for an RRRP.

angle.

The results of the discussion on assembly and working modes are summarised in Table 19.

Input link	Assembly modes	Working modes
Crank	2	1 in each assembly mode
Rocker	2	2 in each assembly mode
π-rocker	1	2
0-rocker	1	2

Table 19. Assembly and working modes.

6. COMPUTING EXTREMA USING DIFFERENTIAL CALCULUS: SINGULARITY ANALYSIS

The slider translation limits always exist since the double point at infinity on the a_3-axis in the v_1-a_3 plane is always an isolated point. However, the existence of $v_{1_{\min/\max}}$ depends on link length conditions. The values for $a_{3_{\min/\max}}$ and $v_{1_{\min/\max}}$, if these exist, can be easily determined using differential calculus, which reveals a completely trigonometry-free classification scheme for the input and output link mobility of planar RRRP linkages.

In addition, $a_{3_{\min/\max}}$ and $v_{1_{\min/\max}}$ are directly linked to determining mechanical and mathematical singularities: singular configurations of the linkage. The study of singular configurations is not trivial and fills numerous articles, books, and also lead to many discussions among kinematicians. They all agree though that if a mechanism approaches a singular configuration, the mechanism becomes uncontrollable because the DOF of the mechanism instantaneously changes, and thus, must be addressed! A mechanical singularity, if it exists, is defined to be a configuration of a mechanism where the subsequent behaviour of the mechanism as it exits the singularity, if it can, is not predictable, or the forces or torques required to leave the singularity become either infinite or nondeterministic.

When the underlying engineering equations of a mechanism or machine are evaluated at the singular

configuration (if any exists), then those equations exhibit mathematical singularity. Singularities can be obtained by examining the tangent space of the IO-equation $F(v_1, a_3) = 0$. Since F is, in general, an n-dimensional implicit function of the input and the output variables, the tangent space can be evaluated by taking the derivative of the IO equation with respect to time and is defined as [40]:

$$\mathbf{J}_{\mathrm{O}}\dot{a_3} + \mathbf{J}_{\mathrm{I}}\dot{v_1} \;=\; 0, \tag{65}$$

where

$$\mathbf{J}_{\mathrm{O}} \;=\; \frac{\partial F}{\partial a_3}, \text{ and } \mathbf{J}_{\mathrm{I}} \;=\; \frac{\partial F}{\partial v_1}. \tag{66}$$

The determinants of the input Jacobian $\mathbf{J}_{\mathrm{I}}$ and the output Jacobian $\mathbf{J}_{\mathrm{O}}$ can be used to classify the linkage's singular configurations. There are three different singularity groups.

1. If $\det(\mathbf{J}_{\mathrm{I}}) = 0$ the linkage is in an **input singularity**, also referred to an inverse-kinematics singularity. For a serial robot arm this occurs at the workspace boundary where the arm is completely stretched out. In the example of the RRRP, it can be used to determine $a_{3_{\min/\max}}$. In this position the linkages loses one, or more, degrees of freedom and is said to be *locked*.

2. If $\det(\mathbf{J}_{\mathrm{O}}) = 0$ the linkage is in an **output singularity**, also referred to direct-kinematics singularity. This configuration occurs when the input link is at a dead-point where the rotation of the input link must change direction. Thus, in the example of the RRRP, it can be used to determine $v_{1_{\min/\max}}$. In this configuration the linkage gains a degree of freedom.

3. If both $\det(\mathbf{J}_{\mathrm{I}}) = 0$ and $\det(\mathbf{J}_{\mathrm{O}}) = 0$ the linkage is in a **combined singularity**. This typically requires special link lengths.

6.1. Computing $v_{1_{\mathrm{crit}}}$ to Determine $a_{3_{\min/\max}}$: Input Singularity

To determine $a_{3_{\min/\max}}$ we must first determine the critical values of v_1 which will be labelled as $v_{1_{\mathrm{crit}}}$. Solving the RRRP algebraic IO equation for a_3 yields two solutions, which are the two working modes within each assembly mode:

$$a_3 \;=\; \frac{(2a_1v_1) \pm \sqrt{-\left((a_1-a_2+a_4)v_1^2 - a_1 - a_2 + a_4\right)\left((a_1+a_2+a_4)v_1^2 - a_1 + a_2 + a_4\right)}}{v_1^2+1},$$

which can be represented more compactly as

$$a_3 \;=\; \frac{(2a_1v_1) \pm \sqrt{-\left(A_2v_1^2 - B_1\right)\left(A_1v_1^2 - B_2\right)}}{v_1^2+1}. \tag{67}$$

Now our algebraic IO equation is expressed as $a_3 = f(v_1)$. The minimum and maximum values for a_3 are obtained by computing the critical values $v_{1_{\mathrm{crit}}}$ of Equation (67). These critical values, if they exist, cause the derivative of a_3 with respect to v_1 to vanish:

$$\frac{\partial a_3}{\partial v_1} \;=\; 0. \tag{68}$$

The symbolic form of this derivative results in a very large and cumbersome expression which can be easily computed using a computer algebra software, such as Maple, but it is not of any utility to display it here. Rather, the values of v_1 that cause Equation (68) to be true are what is important. They are generally called

the *critical values* of the function in Equation (67). The critical value equations of $v_{1_{\text{crit}}}$ for Equation (68) were computed using Maple, but could be obtained by hand with skill, determination, and patience; they are:

$$v_{1_{\text{crit}_1}} = \pm\frac{\sqrt{(a_1+a_2+a_4)(a_1+a_2-a_4)}}{a_1+a_2+a_4} = \pm\frac{\sqrt{A_1B_1}}{A_1}; \tag{69}$$

$$v_{1_{\text{crit}_2}} = \pm\frac{\sqrt{(a_1-a_2+a_4)(a_1-a_2-a_4)}}{a_1-a_2+a_4} = \pm\frac{\sqrt{A_2B_2}}{A_2}. \tag{70}$$

Equation (67) for any particular assemblable and movable RRRP mechanism will evaluate to extreme values of a_3 at $v_{1_{\text{crit}}}$ as $a_{3_{\text{min/max}}} = f(v_{1_{\text{crit}}})$. Because the double point at infinity on the a_3-axis in the v_1-a_3 plane is isolated (an acnode) then at least one of the critical values of v_1 from Equations (69) or (70) must always exist (in other words, be real numbers): $v_{1_{\text{crit}_1}}$ and $v_{1_{\text{crit}_2}}$ cannot simultaneously be complex (imaginary numbers where the radicand is less than zero). Consider the radicands in each equation. Depending on the signed link lengths $\pm a_1$, $\pm a_2$, and $\pm a_4$, it can be shown that the radicands of $\sqrt{A_1B_1}$ and $\sqrt{A_2B_2}$ cannot simultaneously be complex.

Consider for a moment only positive link lengths. Clearly, the factor A_1 must be greater than zero. Moreover, if $B_1 < 0$ then $a_4 > a_1 + a_2$ resulting in a linkage that can't be assembled, see Figure 27. In fact, $B_1 > 0$ represents the *validity condition* for positive link lengths stating that for an assemblable and moveable planar RRRP linkage it must be that

$$a_4 < a_1 + a_2. \tag{71}$$

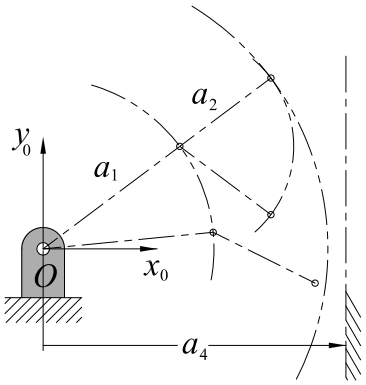

Fig. 27. An unassemblable RRRP because $a_4 > a_1 + a_2$.

However, in the general case the link lengths are directed line segments: their values can be positive or negative. The slider offset distance a_4 can additionally be identically zero. The conclusion is that all four linear factors of the IO curve, A_1, A_2, B_1, and B_2, must be used to determine and classify the mobility of the mechanism.

6.2. Computing $a_{3_{\text{crit}}}$ to Determine $v_{1_{\text{min/max}}}$: Output Singularity

The classification scheme for the angular displacement limits of the input link a_1 depends on the critical values of a_3, abstractly labelled as $a_{3_{\text{crit}}}$. We shall see that these angular limits for the input angle parameter $v_{1_{\text{min/max}}}$, if they exist, depend only on the numerical values of the four linear factors A_1, A_2, B_1, and B_2

which can be either positive, zero, or negative. If the algebraic IO curve possesses no vertical tangents then input link joint angle limits do not exist. To identify the critical values of a_3 we must first solve the RRRP algebraic IO equation for v_1, rearranging the algebraic IO equation as the function $v_1 = f(a_3)$. There are two solutions, which represent the two possible assembly modes of the mechanism:

$$v_1 = \frac{(2a_1a_3) \pm \sqrt{-(a_1^2+a_2^2-a_3^2-a_4^2+2a_1a_2)(a_1^2+a_2^2-a_3^2-a_4^2-2a_1a_2)}}{a_1^2+2a_1a_4-a_2^2+a_3^2+a_4^2}. \quad (72)$$

We now equate the partial derivative of v_1 with respect to a_3 to zero:

$$\frac{\partial v_1}{\partial a_3} = 0. \quad (73)$$

The critical value equations are:

$$a_{3_{\text{crit}_1}} = \pm\sqrt{(a_1+a_2+a_4)(a_1-a_2-a_4)} = \pm\sqrt{A_1B_2}; \quad (74)$$

$$a_{3_{\text{crit}_2}} = \pm\sqrt{(a_1-a_2+a_4)(a_1+a_2-a_4)} = \pm\sqrt{A_2B_1}. \quad (75)$$

If the critical values of a_3 exist then the angular displacement limits of the input link are computed as $v_{1_{\text{min/max}}} = f(a_{3_{\text{crit}}})$. It is to be seen that the existence of $a_{3_{\text{crit}}}$ requires either, or both, of Equations (74) and (75) to be real valued.

6.3. Examples

We will now compute the extrema for the a_1 input link angles and the a_3 slider translation for different types of IO curve. This novel solution technique reveals the extrema of both working modes in each assembly mode, something which, the best knowledge of the authors, is not to be found in the existing literature with the exception of [40]. In that paper the author use the derivatives of the trigonometric form of the input-output correlation, they do not to explicitly identify the assembly and working mode solutions, rather only the forward kinematics solutions.

6.3.1. Crank

The extrema for the crank IO curve illustrated in Figure 28a will now be computed: the link lengths are $a_1 = 1$, $a_2 = 4$, and $a_4 = 2$. Observe that the curve possesses no vertical tangents, hence there this crank has two assembly modes, but only one working mode in each. To obtain the critical values of v_1 we obtain the function $a_3 = f(v_1)$:

$$a_3 = \frac{2v_1 + \pm\sqrt{7v_1^4+26v_1^2+15}}{v_1^2+1}. \quad (76)$$

Next, the partial derivative $\partial a_3/\partial v_1$ is computed, equated to zero, and solved for $v_{1_{\text{crit}}}$ yielding solutions for each assembly mode (note, linkages of this type have two assembly modes but onle one working mode in each):

$$v_{1_{\text{crit}_1}} = -2.236067977,\ 0.6546536709; \quad (77)$$

$$v_{1_{\text{crit}_2}} = 2.236067977,\ -0.6546536709. \quad (78)$$

The corresponding four limiting values of a_3 are obtained by back substituting the values of $v_{1_{\text{crit}}}$ into Equation (76). In this case, the computed values of $a_{3_{\text{min}}}$ and $a_{3_{\text{max}}}$ in each assembly mode has an associated

value for a_3 in the opposite assembly mode. This unexpected algebraic behaviour is explicitly revealed by $v_{1_{\text{crit}}}$. The limiting values are listed in Table 20, and illustrated in Figure 28. Note that in the figure the two assembly modes are abbreviated as "AM1" and "AM2", while the associated values for a_3 in the opposite assembly modes are abbreviated as "alt".

Upper assembly mode		Lower assembly mode
$a_{3_{\text{min}}}$	2.236067978	-2.236067978
$a_{3_{\text{alt}}}$	-3.726779963	3.726779963
$a_{3_{\text{max}}}$	4.582575695	-4.582575695
$a_{3_{\text{alt}}}$	-2.749545416	2.749545416

Table 20. Slider translation limits.

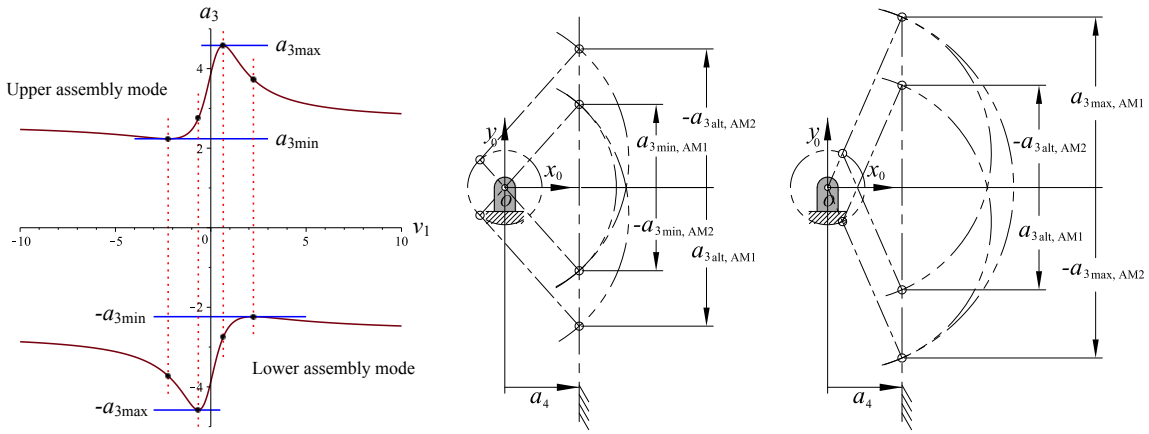

(a) IO curve and critical points for input crank.

(b) Slider translation limits for input crank.

Fig. 28. Crank-slider with $a_1 = 1$, $a_2 = 4$, and $a_4 = 2$: **two assembly modes with one working mode in each**.

Since the input link in this mechanism is designed to be a crank, then clearly there will be no input joint angle parameter limits $v_{1_{\text{min/max}}}$. Still, in the interest of rigour we will now attempt to identify $a_{3_{\text{crit}}}$ by solving the crank IO equation for v_1 leading to

$$v_1 = \frac{2a_3 \pm \sqrt{-a_3^4 + 26a_3^2 - 105}}{a_3^2 - 7}. \tag{79}$$

Next, compute the partial derivative $\partial v_1/\partial a_3 = 0$ and solve for $a_{3_{\text{crit}}}$. The solutions evaluate to

$$a_{3_{\text{crit}}} = \begin{cases} \pm 5.916079783\, i, \\ \pm 1.732050808\, i. \end{cases} \tag{80}$$

We conclude that there are no input joint angle limits. Moreover, in general we can conclude that if there are no real values for $a_{3_{\text{crit}}}$ then the input link will always be a crank. In this case the linear coefficient factors A_2 and B_2 are both less than zero:

$$\begin{aligned} A_2 &= a_1 - a_2 - a_4 = 1 - 4 - 2 = -5 < 0; \\ B_2 &= a_1 - a_2 + a_4 = 1 - 4 + 2 = -1 < 0. \end{aligned}$$

Hence, both conditions in Equations (74) and (75) evaluate to complex (imaginary) numbers:

$$a_{3_{\text{crit}_1}} = \pm\sqrt{A_1 B_2} = \pm\sqrt{(7)(-5)} = \sqrt{-35} = \pm 5.916079783\, i;$$

$$a_{3_{\text{crit}_2}} = \pm\sqrt{A_2 B_1} = \pm\sqrt{(-1)(3)} = \pm\sqrt{-3} = \pm 1.732050808\, i.$$

6.3.2. π-rocker

We can create a π-rocker with the link lengths $a_1 = 3$, $a_2 = 2$, and $a_4 = -4$. The algebraic IO equation for this mechanism, illustrated in Figure 29, is expressed in the form $a_3 = f(v_1)$ as:

$$a_3 = \frac{6v_1 \pm \sqrt{3v_1^4 - 6v_1^2 - 45}}{v_1^2 + 1}. \tag{81}$$

The partial derivative $\partial a_3/\partial v_1$ is computed, equated to zero, and solved for $v_{1_{\text{crit}}}$ yielding solutions for each working mode:

$$v_{1_{\text{crit}_1}} = \pm 3; \tag{82}$$

$$v_{1_{\text{crit}_2}} = \pm 1.290994449\, i. \tag{83}$$

We find that $v_{1_{\text{crit}_1}}$ is real-valued while $v_{1_{\text{crit}_2}}$ is complex because the linear factor $A_2 < 0$. Back substituting the values for $v_{1_{\text{crit}}}$ into Equation (81) reveals the slider translation limits in both working modes (note, this type of linkage has only one assembly mode) listed in Table 21. These values require a bit of explanation. The absolute slider displacement limits are indeed $a_{3_{\text{min/max}}}$ are indeed ± 3. However, the other values of $\pm 3/5$ are not the min/max values in the opposite working mode, rather they are the alternate values of a_3 that result from the critical values for v_1.

Upper working mode		Lower working mode
$a_{3_{\text{max/min}}}$	3	-3
$a_{3_{\text{alt}}}$	3/5	-3/5

Table 21. Slider translation limits for input π-rocker.

The π-rocker-slider IO curve and the linkage that generates it are illustrated in Figures 29 and 30. By design, this linkage is a π-rocker-slider and hence the input link rocks between $\pm\theta_{1_{\text{min}}}$, there are no values for $\pm\theta_{1_{\text{max}}}$. So, there will be at most two of four values for $a_{3_{\text{crit}}}$ obtained by solving the IO equation for $v_1 = f(a_3)$

$$v_1 = \frac{6a_3 \pm \sqrt{-a_3^4 - 6a_3^2 + 135}}{a_3^2 - 3}. \tag{84}$$

The partial derivative $\partial v_1/\partial a_3 = 0$ must now be solved, revealing

$$a_{3_{\text{crit}_{1,\,2}}} = \pm 2.236067977,\ \pm 5.196152424\, i.$$

The reason that $a_{3_{\text{crit}_2}}$ is a complex number is because the link lengths cause the linear factor A_2 to be less than zero:

$$A_2 = a_1 - a_2 + a_4 = 3 - 2 - 4 = -3 < 0,$$

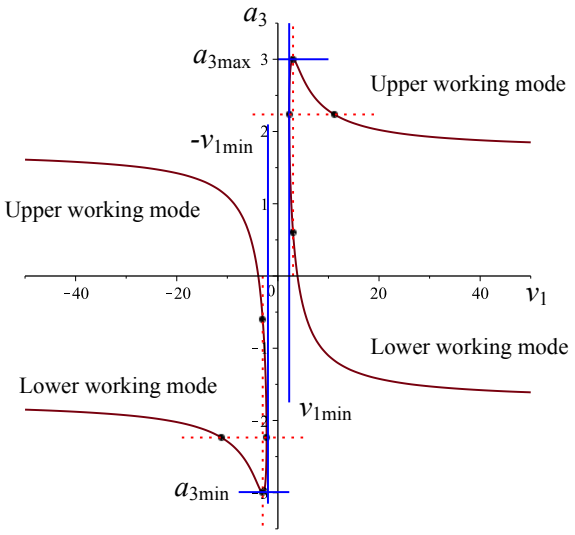

Fig. 29. IO curve and critical points for input π-rocker.

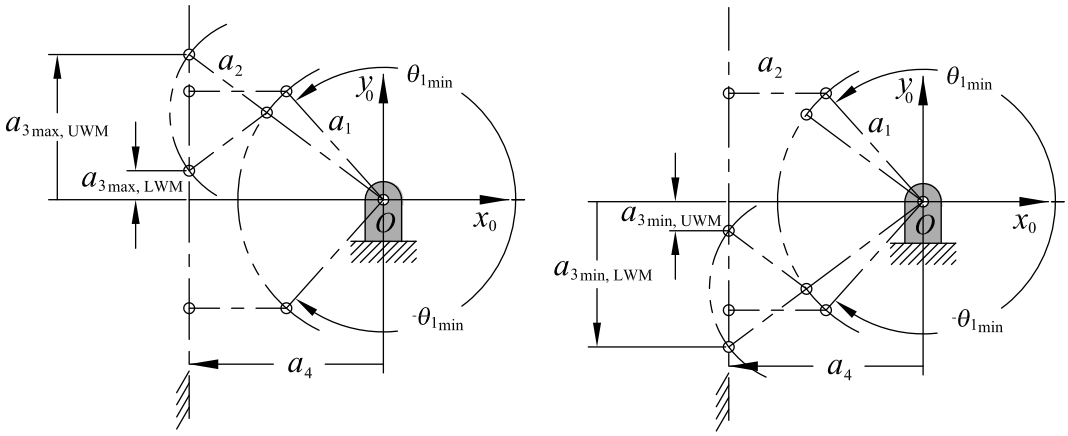

Fig. 30. π-rocker-slider with $a_1 = 3$, $a_2 = 2$, and $a_4 = -4$: **one assembly mode with two working modes**.

so that

$$a_{3_{\text{crit}_2}} = \pm\sqrt{A_2 B_1} = \pm\sqrt{(-3)(9)} = \pm\sqrt{-27} = \pm 5.196152424\, i.$$

The real values for the input link minimum angle parameter $\pm v_{1_{\text{min}}}$ as well as $\pm v_{1_{\text{alt}}}$ (and therefore input angle limits angle $\pm\theta_{\text{min}}$ as well as $\pm\theta_{\text{alt}}$) are revealed by substituting the two real values for $a_{3_{\text{crit}}}$ into Equation (84):

$$\begin{aligned} v_{1_{\text{min}}} &= \pm 2.236067978; \\ v_{1_{\text{alt}}} &= \pm 11.18033990; \\ \theta_{1_{\text{min}}} &= \pm 131.8103149^\circ; \\ \theta_{1_{\text{alt}}} &= \pm 169.7778205^\circ. \end{aligned}$$

The second solution for $\theta_{1_{\text{alt}}} = \pm 169.7778205^\circ$ exists, but does not correspond to an input angle extreme, see Figure 29.

6.3.3. 0-rocker

We will create a 0-rocker that is just the previous π-rocker mirrored in the y_0-axis, therefore it has link lengths $a_1 = 3$, $a_2 = 2$, and $a_4 = 4$. The 0-rocker-slider IO curve and the linkage that generates it are illustrated in Figure 31. The algebraic IO equation for this mechanism is expressed in the form $a_3 = f(v_1)$ as:

$$a_3 = \frac{6v_1 \pm \sqrt{-45v_1^4 - 6v_1^2 + 3}}{v_1^2 + 1}. \tag{85}$$

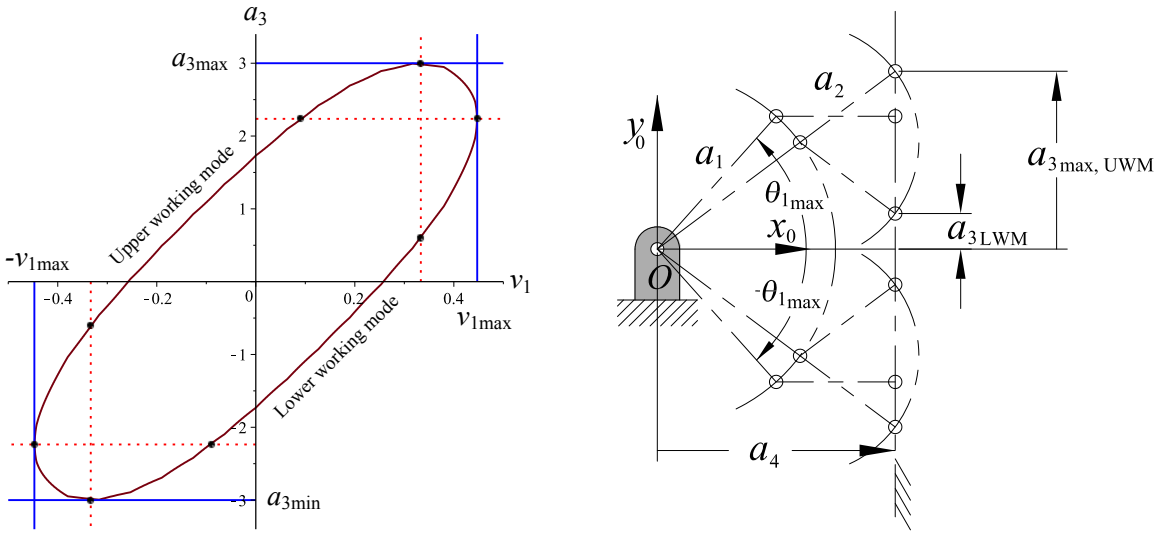

(a) IO curve and critical points for input 0-rocker.

(b) Slider translation limits for input 0-rocker.

Fig. 31. 0-rocker-slider with $a_1 = 3$, $a_2 = 2$, and $a_4 = 4$: **one assembly mode with two working modes**.

The partial derivative $\partial a_3/\partial v_1$ is computed, equated to zero, and solved for $v_{1_{\text{crit}}}$ yielding solutions for each working mode:

$$v_{1_{\text{crit}_1}} = \pm\frac{1}{3}; \tag{86}$$

$$v_{1_{\text{crit}_2}} = \pm 0.774596669\, i. \tag{87}$$

As for the π-rocker, we find that $v_{1_{\text{crit}_1}}$ is real-valued while $v_{1_{\text{crit}_2}}$ is complex, but in this case, because the linear factor $B_2 < 0$. Back substituting these values for $v_{1_{\text{crit}}}$ into Equation (85) reveals the slider translation limits in both working modes (note, this type of linkage has only one assembly mode) listed in Table 22. These values require a bit of explanation. The absolute slider displacement limits are indeed $a_{3_{\text{min/max}}}$ are indeed ± 3. However, the other values of $\pm 3/5$ are not the min/max values in the opposite working mode, rather they are the alternate values of a_3 that result from the critical values for v_1.

By design, this linkage is a 0-rocker-slider and hence the input link rocks between $\pm\theta_{1_{\max}}$, there are no values for $\pm\theta_{1_{\min}}$. So, there will be at most two of four values for $a_{3_{\text{crit}}}$ obtained by solving the IO equation for $v_1 = f(a_3)$

$$v_1 = \frac{6a_3 \pm \sqrt{-a_3^4 - 6a_3^2 + 135}}{a_3^2 + 45}. \tag{88}$$

Upper working mode		Lower working mode
$a_{3_{\max/\min}}$	3	3
$a_{3_{\text{alt}}}$	3/5	-3/5

Table 22. Slider translation limits for input 0-rocker.

The partial derivative $\partial v_1/\partial a_3 = 0$ must now be solved, revealing

$$a_{3_{\text{crit}_{1,\,2}}} \;=\; \mp 5.196152424\,i,\;\; \pm 2.236067977.$$

The reason that $a_{3_{\text{crit}_1}}$ is a complex number is because the link lengths cause the linear factor B_2 to be less than zero:

$$B_2 \;=\; a_1 - a_2 - a_4 \;=\; 3-2-4 \;=\; -3 \;<\; 0,$$

so that

$$a_{3_{\text{crit}_1}} \;=\; \pm\sqrt{A_1 B_2} \;=\; \pm\sqrt{(9)(-3)} \;=\; \pm\sqrt{-27} \;=\; \pm 5.196152424\,i.$$

The real values for the input link minimum angle parameter $\pm v_{1_{\max}}$ as well as $\pm v_{1_{\text{alt}}}$ (and therefore input angle limits angle $\pm\theta_{\max}$) are revealed by substituting the two real values for $a_{3_{\text{crit}}}$ into Equation (88):

$$\begin{aligned} v_{1_{\max}} &= \pm 0.4472135954; \\ v_{1_{\text{alt}}} &= \pm 0.08944271904; \\ \theta_{1_{\max}} &= \pm 48.18968509^\circ; \\ \theta_{1_{\text{alt}}} &= \pm 10.22217938^\circ. \end{aligned}$$

The second solution for $\theta_{1_{\text{alt}}} = \pm 10.22217938^\circ$ exists, but does not correspond to an input angle extreme, see Figure 31a.

6.3.4. Rocker

Finally, we will create a rocker that has link lengths $a_1 = 6$, $a_2 = 1$, and $a_4 = 2$. The rocker-slider IO curve and the linkage that generates it are illustrated in Figures 32a and 32b. The algebraic IO equation for this mechanism is expressed in the form $a_3 = f(v_1)$ as:

$$a_3 \;=\; \frac{12v_1 \pm \sqrt{-63v_1^4 + 66v_1^2 - 15}}{v_1^2 + 1}. \tag{89}$$

The partial derivative $\partial a_3/\partial v_1$ is computed, equated to zero, and solved for $v_{1_{\text{crit}}}$ yielding solutions for each working mode:

$$v_{1_{\text{crit}_1}} \;=\; \pm 0.7453559923; \tag{90}$$

$$v_{1_{\text{crit}_2}} \;=\; \pm 0.6546536709. \tag{91}$$

As opposed to the π- and 0-rockers, we find that $v_{1_{\text{crit}_1}}$ and $v_{1_{\text{crit}_2}}$ are both real-valued. Back substituting these values for $v_{1_{\text{crit}}}$ into Equation (89) reveals the slider translation limits in both assembly and working modes listed in Table 23.

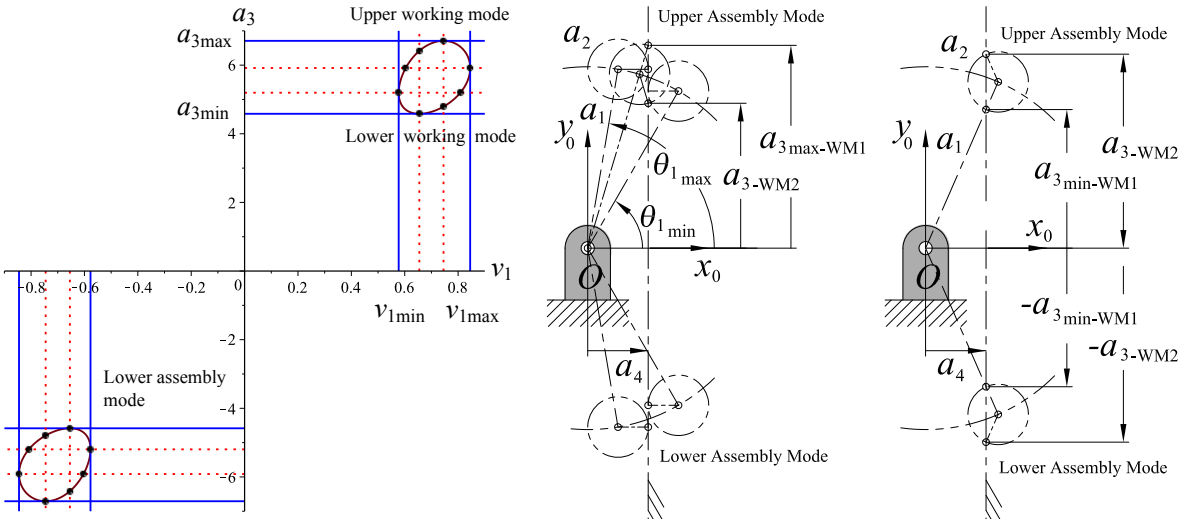

(a) IO curve and critical points for input rocker.

(b) Slider translation limits for input rocker.

Fig. 32. Rocker-slider with $a_1 = 6$, $a_2 = 1$, and $a_4 = 2$: **two assembly modes with two working modes in each**.

Upper assembly mode	Upper working mode	Lower working mode
$a_{3_{\max/\min}}$	6.708203948	4.582575697
$a_{3_{\text{alt}}}$	4.791574227	6.415605970
Lower assembly mode	Upper working mode	Lower working mode
$a_{3_{\max/\min}}$	-6.708203948	-4.582575697
$a_{3_{\text{alt}}}$	-4.791574227	-6.415605970

Table 23. Slider translation limits for input rocker.

By design, this linkage is a rocker-slider and hence the input link rocks between $\pm\theta_{1_{\max}}$ and $\pm\theta_{1_{\min}}$. So, there must be four values for $a_{3_{\text{crit}}}$ obtained by solving the IO equation for $v_1 = f(a_3)$

$$v_1 = \frac{12a_3 \pm \sqrt{-a_3^4 + 66a_3^2 - 945}}{a_3^2 + 63}. \tag{92}$$

The partial derivative $\partial v_1/\partial a_3 = 0$ must now be solved, revealing

$$a_{3_{\text{crit}_{1,2}}} = \pm 5.916079783,\ \pm 5.196152424.$$

The real values for the input link limiting angle parameters $\pm v_{1_{\min/\max}}$ (and therefore input angle limits angle $\pm\theta_{\min/\max}$) are revealed by substituting the values for $a_{3_{\text{crit}}}$ into Equation (92):

$$\left.\begin{array}{llll} v_{1_{\max}} = \pm 0.84515425, & v_{1_{\max-\text{alt}}} = \pm 0.6036816104; \\ \theta_{1_{\max}} = \pm 80.40593176^\circ, & \theta_{1_{\max-\text{alt}}} = \pm 62.23721622^\circ; \\ v_{1_{\min}} = \pm 0.5773502683, & v_{1_{\min-\text{alt}}} = \pm 0.8082903782; \\ \theta_{1_{\min}} = \pm 60^\circ, & \theta_{1_{\min-\text{alt}}} = \pm 77.89655121^\circ. \end{array}\right\} \tag{93}$$

The second solutions for $\theta_{1_{\max-\text{alt}}} = \pm 62.23721622^\circ$ and $\theta_{1_{\min-\text{alt}}} = \pm 77.89655121^\circ$ both exist, but do not correspond input angle extremes, see Figure 32a.

The observations based on the results of the preceding four examples are listed in Table 24.

	Input link	$v_{1_{\text{crit}_1}} = \pm\frac{\sqrt{A_1 B_1}}{A_1}$	$v_{1_{\text{crit}_2}} = \pm\frac{\sqrt{A_2 B_2}}{A_2}$	$a_{3_{\text{crit}_1}} = \pm\sqrt{A_1 B_2}$	$a_{3_{\text{crit}_2}} = \pm\sqrt{A_2 B_1}$	Angle limit
1.	Crank	$\mathbb{R}$	$\mathbb{R}$	$\mathbb{C}$	$\mathbb{C}$	None
2.	NA	$\mathbb{C}$	$\mathbb{R}$	$\mathbb{C}$	$\mathbb{C}$	NA
3.	NA	$\mathbb{R}$	$\mathbb{C}$	$\mathbb{C}$	$\mathbb{C}$	NA
4.	NA	$\mathbb{C}$	$\mathbb{C}$	$\mathbb{C}$	$\mathbb{C}$	NA
5.	Rocker	$\mathbb{R}$	$\mathbb{R}$	$\mathbb{R}$	$\mathbb{R}$	$\pm\theta_{1_{\min/\max}}$
6.	NA	$\mathbb{C}$	$\mathbb{R}$	$\mathbb{R}$	$\mathbb{R}$	NA
7.	NA	$\mathbb{R}$	$\mathbb{C}$	$\mathbb{R}$	$\mathbb{R}$	NA
8.	NA	$\mathbb{C}$	$\mathbb{C}$	$\mathbb{R}$	$\mathbb{R}$	NA
9.	NA	$\mathbb{R}$	$\mathbb{C}$	$\mathbb{R}$	$\mathbb{R}$	NA
10.	NA	$\mathbb{R}$	$\mathbb{C}$	$\mathbb{C}$	$\mathbb{C}$	NA
11.	NA	$\mathbb{C}$	$\mathbb{R}$	$\mathbb{R}$	$\mathbb{R}$	NA
12.	NA	$\mathbb{C}$	$\mathbb{R}$	$\mathbb{C}$	$\mathbb{C}$	NA
13.	π-rocker	$\mathbb{R}$	$\mathbb{C}$	$\mathbb{R}$	$\mathbb{C}$	$\pm\theta_{1_{\min}}$
14.	0-rocker	$\mathbb{R}$	$\mathbb{C}$	$\mathbb{C}$	$\mathbb{R}$	$\pm\theta_{1_{\max}}$
15.	0-rocker	$\mathbb{C}$	$\mathbb{R}$	$\mathbb{R}$	$\mathbb{C}$	$\pm\theta_{1_{\max}}$
16.	π-rocker	$\mathbb{C}$	$\mathbb{R}$	$\mathbb{C}$	$\mathbb{R}$	$\pm\theta_{1_{\min}}$

Table 24. Complete input link mobility classification: $\mathbb{R}$ = real number; $\mathbb{C}$ = complex number; NA = not assemblable.

7. COUPLER POINT CURVES

One of the earliest recorded examples of mechanical system design for guiding a point along a curve belongs to Archimedes (ca. 287-212 BC). He was born in Syracuse in the ancient Greek colony of Sicily, but he studied mathematics at the Museum in Alexandria [3] between 250-240 BC under the direction of Conon of Samos. Conon was a mathematician who was a pupil of Euclid and became the custodian of the library of Alexandria after Euclid's death. Archimedes work is the first recorded systematic study of mechanism design and analysis, although undoubtedly these concepts were widely studied earlier everywhere there were humans who could formulate abstract thoughts. However, the very first patent [7] for a mechanism designed to move a point along a desired curve belongs to James Watt (1736-1819) awarded more than 2000 years after Archimedes death.

7.1. Planar 4R Coupler Point Curves

The coupler point curve for an arbitrary planar 4R mechanism is geometrically very rich. An arbitrary point on the coupler, which will be called Point C, is constrained by the fact that two of the coupler's points move on the fixed-centred circles described by the motions of the input and output links, see Figure 33.

The curve traced by point C is, in general, a curve of degree 6, bearing the formidable name of *tri-circular sextic*, see [27] for a full explanation of what this name means. But briefly, because two of the coupler points move on circles it turns out that every planar 4R coupler curve possesses the same three pairs of complex conjugate multiple points at infinity which are common to every circle.

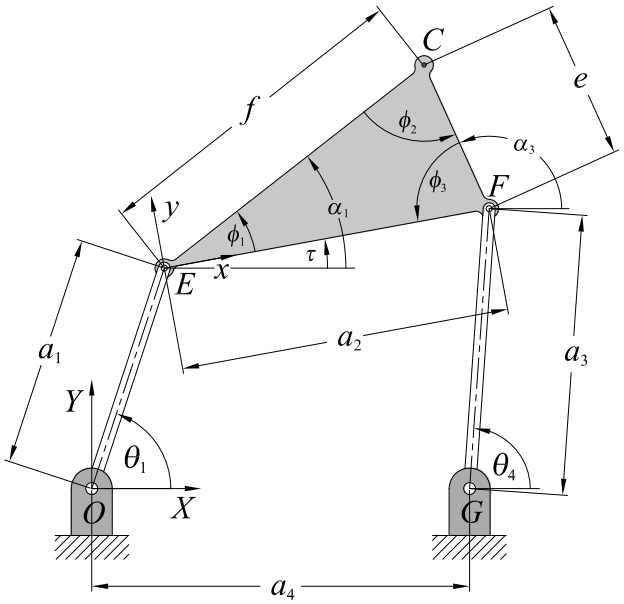

Fig. 33. Planar 4R coupler point geometric parameters.

The following derivation of the coupler point curve of a planar 4R mechanism was devised by Samuel Roberts [41] in 1876. The coordinates of points E and F in the $X-Y$ coordinate system whose origin is located at the centre of the ground-fixed R-pair on the left, see Figure 33, in terms of the location of the coupler point C with coordinates (X_C, Y_C) in the same coordinate system:

$$\mathbf{E} = \begin{bmatrix} X_C - f\cos\alpha_1 \\ Y_C - f\sin\alpha_1 \end{bmatrix}; \tag{94}$$

$$\mathbf{F} = \begin{bmatrix} X_C - e\cos\alpha_3 - a_4 \\ Y_C - e\sin\alpha_3 \end{bmatrix}. \tag{95}$$

Because points E and F move on fixed-centred circles it must be that $\mathbf{E}\cdot\mathbf{E} = a_1^2$ and $\mathbf{F}\cdot\mathbf{F} = a_3^2$, so we can write

$$X_C^2 - 2X_C f\cos(\alpha_1) + f^2 + Y_C^2 - 2Y_C f\sin(\alpha_1) - a_1^2 = 0, \tag{96}$$

and

$$X_C^2 - 2X_C e\cos(\alpha_3) - 2X_C a_4 + e^2 + 2e\cos(\alpha_3)a_4 + a_4^2 + Y_C^2 - 2Y_C e\sin(\alpha_3) - a_3^2 = 0. \tag{97}$$

It will be convenient to express α_3 in terms of α_1 and ϕ_2. For this we can use the triangle interior/exterior angle rule [36]. Consider the triangle illustrated in Figure 34a. Consider that

$$\phi_1 + \phi_2 + \phi_3 = \pi,$$

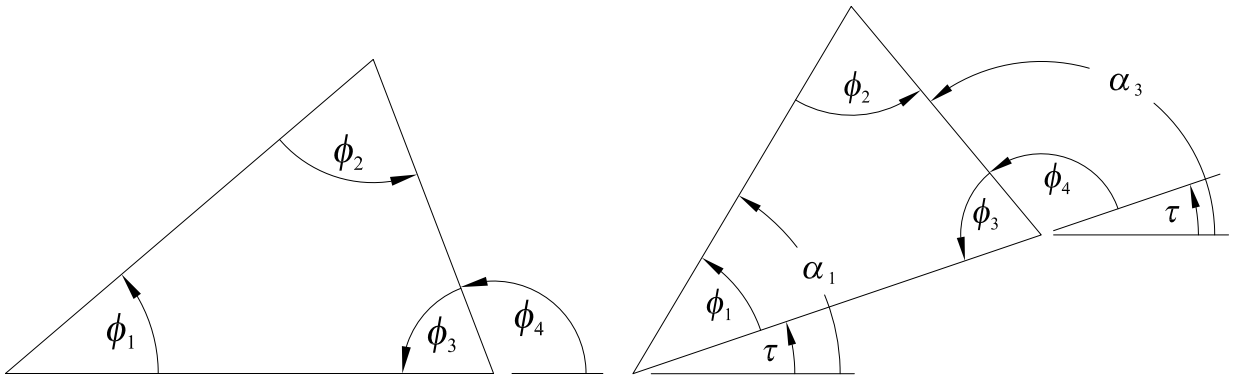

(a) Triangle angle rule.

(b) Triangle angle rule adapted for coupler.

Fig. 34. Triangle angle rules.

and

$$\phi_3 + \phi_4 \quad = \quad \pi.$$

Then we can say that

$$\phi_4 \quad = \quad \pi - \phi_3,$$

and

$$\phi_1 + \phi_2 \quad = \quad \pi - \phi_3.$$

Therefore

$$\phi_1 + \phi_2 \quad = \quad \phi_4. \tag{98}$$

The same rule holds for the triangle shown in Figure 34b, that is τ can be added to both sides of Equation (98) without changing it's validity:

$$\underbrace{(\phi_1 + \tau)}_{\alpha_1} + \phi_2 \quad = \quad \underbrace{(\phi_4 + \tau)}_{\alpha_3}.$$

Therefore

$$\alpha_1 + \phi_2 \quad = \quad \alpha_3. \tag{99}$$

Make this substitution in Equation (97) and use the identity

$$\cos(\alpha_1 + \phi_2) \quad = \quad \cos\alpha_1 \cos\phi_2 - \sin\alpha_1 \sin\phi_2 \tag{100}$$

to separate the angles in the trigonometric arguments giving two equations in $\cos\alpha_1$ and $\sin\alpha_1$:

$$\begin{aligned} S_1 \cos\alpha_1 + T_1 \sin\alpha_1 &= U_1, \\ S_2 \cos\alpha_1 + T_2 \sin\alpha_1 &= U_2, \end{aligned}$$

where

$$\begin{array}{rcl} S_1 &=& 2X_C f, \\ T_1 &=& 2Y_C f, \\ U_1 &=& X_C^2 + Y_C^2 + f^2 - a_1^2. \end{array} \quad \left\| \quad \begin{array}{rcl} S_2 &=& 2e\left((X_C - a_4)\cos\phi_2 - Y_C \sin\phi_2\right), \\ T_2 &=& 2e\left(Y_C \cos\phi_2 - (X_C - a_4)\sin\phi_2\right), \\ U_2 &=& (X_C - a_4)^2 + Y_C^2 + e^2 - a_3^2. \end{array} \right.$$

Arrange these two equations vector-matrix form as

$$\begin{bmatrix} S_1 & T_1 \\ S_2 & T_2 \end{bmatrix} \begin{bmatrix} \cos\alpha_1 \\ \sin\alpha_1 \end{bmatrix} = \begin{bmatrix} U_1 \\ U_2 \end{bmatrix}, \tag{101}$$

and solve Equations (101) for $\cos\alpha_1$ and $\sin\alpha_1$ using Cramer's rule:

$$\cos\alpha_1 = \frac{\begin{vmatrix} U_1 & T_1 \\ U_2 & T_2 \end{vmatrix}}{\begin{vmatrix} S_1 & T_1 \\ S_2 & T_2 \end{vmatrix}} = \frac{U_1 T_2 - U_2 T_1}{S_1 T_2 - S_2 T_1}, \quad \text{and} \tag{102}$$

$$\sin\alpha_1 = \frac{\begin{vmatrix} S_1 & U_1 \\ S_2 & U_2 \end{vmatrix}}{\begin{vmatrix} S_1 & T_1 \\ S_2 & T_2 \end{vmatrix}} = \frac{S_1 U_2 - S_2 U_1}{S_1 T_2 - S_2 T_1}. \tag{103}$$

Finally we enforce the identity $\cos^2\alpha_1 + \sin^2\alpha_1 = 1$ to obtain

$$(U_1 T_2 - U_2 T_1)^2 + (S_1 U_2 - S_2 U_1)^2 = (S_1 T_2 - S_2 T_1)^2,$$

or

$$(U_1 T_2 - U_2 T_1)^2 + (S_1 U_2 - S_2 U_1)^2 - (S_1 T_2 - S_2 T_1)^2 = 0. \tag{104}$$

The S_i and T_i coefficients in Equation (104) are linear functions in the coordinates of the coupler point X_C and Y_C, while the U_i are quadratic. The products $U_i T_j$ and $S_j U_i$ are of degree 3, and the squares of the differences are of order six. Hence, the coupler point curve of an arbitrary planar 4R mechanism represented by Equation (104) is of degree six, a *sextic*, agreeing with the well known theory of planar mechanisms [27].

REFERENCES

1. Hayes, M.J.D., Rotzoll, M. and Husty, M.L. "Design Parameter Space of Planar Four-bar Linkages." Proceedings of the 15^{th} IFToMM World Congress, June 30-July 4, 2019.
2. Hartenberg, R. and Denavit, J. *Kinematic Synthesis of Linkages*. McGraw-Hill, Book Co., New York, N.Y., U.S.A., 1964.
3. Ceccarelli, M. *Distinguished Figures in Mechanism and Machine Science, Their Contributions and Legacies Part 1*. Springer, New York, U.S.A., 2007.
4. Reuleaux, F. *The Kinematics of Machinery: Outlines of a Theory of Machines,* Translated and Edited by A.B.W. Kennedy. MacMillan and Co., 1876.
5. Freudenstein, F. "Approximate Synthesis of Four-Bar Linkages." *Trans. ASME*, Vol. vol 77, pp. 853–861, 1955.
6. Burmester, L. *Lehrbuch der Kinematik*. Arthur Felix Verlag, Leipzig, Germany, 1888.
7. Watt, J. "Patent No. 1432, April 28, 1784.", 1784.
8. Uicker, J.J., Pennock, G.R. and Shigley, J.E. *Theory of Machines and Mechanisms,* 5^{th} edition. Oxford University Press, New York, N.Y., U.S.A., 2017.

9. Cipolla, R. and Giblin, P. *Visual Motion of Curves and Surfaces*. Cambridge University Press, Cambridge, U.K., 2000.
10. Kreyszig, E. *Differential Geometry*. Dover Publications, Inc., New York, N.Y., U.S.A., 1991.
11. Freudenstein, F. "An Analytical Approach to the Design of Fourlink Mechanisms." *Trans. ASME*, Vol. vol 77, pp. 483–492, 1954.
12. Hayes, M.J.D., Husty, M.L. and Pfurner, M. "Input-output Equation for Planar Four-bar Linkages." pp. 12–19. *16th Advances in Robotic Kinematics*, eds. Lenarčič, J. and Parenti-Castelli, V., Springer, New York, 2018.
13. Husty, M.L. and Pfurner, M. "An Algebraic Version of the Input-Output Equation of Planar Four-Bar Mechanisms." pp. 746–757. *International Conference on Geometry and Graphics*, Milan, Italy, 2018.
14. Rotzoll, M., Hayes, M.J.D., Husty, M.L. and Pfurner, M. "A General Method for Determining Algebraic Input-output Equations for Planar and Spherical 4R Linkages." *17th International Symposium: Advances in Robotic Kinematics*, Ljubljana, Slovenia, June 28-July 2, 2020.
15. Denavit, J. and Hartenberg, R.S. "A Kinematic Notation for Lower-pair Mechanisms Based on Matrices." *Trans ASME J. Appl. Mech.*, Vol. 23, p. 215–221, 1955.
16. Study, E. *Geometrie der Dynamen*. Teubner Verlag, Leipzig, Germany, 1903.
17. Adams, W. and Loustaunau, P. *An Introduction to Gröbner Bases*, Vol. 3. American Mathematical Society, Graduate Studies in Mathematics, 1994.
18. Cox, D., Little, J. and O'Shea, D. *Ideals, Varieties, and Algorithms: an Introduction to Computational Algebraic Geometry and Commutative Algebra,* second edition. Springer-Verlag, Berlin, Germany, 1997.
19. Rotzoll, M., Hayes, M.J.D. and Husty, M.L. "An Algebraic Input-Output Equation for Planar RRRP and PRRP Linkages." *Proceedings of the 10th CCToMM Symposium on Mechanisms, Machines, and Mechatronics*, École de technologie supérieure, Montréal, QC, Canada, May 16-17, 2019.
20. Rotzoll, M. and Hayes, M.J.D. "A General Method for Determining Algebraic Input-output Equations for the Slider-crank and the Bennett Linkage." *11th CCToMM Symposium on Mechanisms, Machines, and Mechatronics*, Ontario Tech University, Oshawa, ON, Canada, June 3-4, 2021.
21. Hayes, M.J.D., Rotzoll, M., Ingalls, C. and Pfurner, M. "Design Parameter Space of Spherical Four-bar Linkages." Proceedings of *EuCoMeS 2020, 8th European Conference on Mechanism Science*, Cluj-Napoca, Romania, September 7-10, 2020.
22. Coxeter, H.S.M. *Regular Polytopes, 3rd Edition*. Dover Publications, Inc., New York, N.Y., U.S.A., 1973.
23. Coxeter, H.S.M. *Projective Geometry,* second edition. University of Toronto Press, Toronto, On., Canada, 1974.
24. McCarthy, J.M. "Planar and Spatial Rigid Motion as Special Cases of Spherical and 3-Spherical Motion." *Journal of Mechanisms, Transmissions, and Automation in Design*, Vol. 105, No. 3, pp. 569–575, 1983.
25. Segre, B. *The Non-singular Cubic Surfaces; a New Method of Investigation with Special Reference to Questions of Reality*. Oxford, The Clarendon Press, 1942.
26. Rotzoll, M., Bucciol, Q. and Hayes, M.J.D. "Algebraic Input-output Angle Equation Derivation Algorithm for the Six Distinct Angle Pairings in Arbitrary Planar 4R Linkages." Submitted to *20th International Conference on Advanced Robotics, ICAR 2021*, Ljubljana, Slovenia, December 6-10, 2021.
27. Hunt, K. *Kinematic Geometry of Mechanisms*. Clarendon Press, Oxford, England, 1978.
28. Salmon, G. *A Treatise on the Higher Plane Curves,* third edition. Hodges, Foster, and Figgis, Dublin, Rep. of Ireland, 1879.
29. Sachs, H. *Comett II, Modul II: Linengeometrie*, Manuskript, Leoben, Austria, 1993.
30. Husty, M., Karger, A., Sachs, H. and Steinhilper, W. *Kinematik und Robotik*. Springer-Verlag, Berlin, Germany, 1997.
31. Freudenstein, F. "On the Maximum and Minimum Velocities and the Accelerations in Four-link Mechanisms." *Trans. ASME*, Vol. 78, pp. 779–787, 1956.
32. Wu, L.I. and Wu, S.H. "A Note on Freudenstein's Theorem." *Mechanism and Machine Theory*, Vol. vol 33, No. 1/2, pp. 139–149, 1998.
33. Hall, A.S. *Kinematics and Linkage Design*. Prentice-Hall, Inc., Englewood Cliffs, N.J., U.S.A., 1961.
34. McCarthy, J.M. and Soh, G.S. *Geometric Design of Linkages, 2nd Edition* Interdiciplinaty Applied Mathematics. Springer, New York, N.Y., 2011.
35. Hayes, M.J.D., Rotzoll, M., Iraei, A., Nichol, A. and Bucciol, Q. "Algebraic Differential Kinematics of Planar 4R Linkages." Submitted to *20th International Conference on Advanced Robotics, ICAR 2021*, Ljubljana, Slovenia, December 6-10, 2021.

36. Euclid. *The Thirteen Books of the Elements,* second edition, translation by Sir T. L. Heath, vol's 1,2,3. Dover Publications, Inc., New York, N.Y., U.S.A., 1956.
37. Chebyshev, P.L. *Théorie des méchanismes connus sous le nom de parallélogrammes (1853) from "Oeuvres de P.L. Tchebychef"*. Markoff et Sonin, 1899.
38. Hayes, M.J.D., Parsa, K. and Angeles, J. "The Effect of Data-Set Cardinality on the Design and Structural Errors of Four-Bar Function-Generators." *Proceedings of the Tenth World Congress on the Theory of Machines and Mechanisms,* Oulu, Finland*, pages 437-442*, 1999.
39. Guigue, A. and Hayes, M.J.D. "Continuous Approximate Synthesis of Planar Function-generators Minimising the Design Error." *Mechanism and Machine Theory*, Vol. 101, pp. 158–167, DOI: 10.1016/j.mechmachtheory.2016.03.012, 2016.
40. Gosselin, C.M. and Angeles, J. "Singularity Analysis of Closed-loop Kinematic Chains." *IEEE Transactions on Robotics and Automation*, Vol. 6, No. 3, p. 281–290, 1990.
41. Roberts, S. "On Three-bar Motion in Plane Space." *Proc. London Math. Soc.*, Vol. 7, pp. 286–318, 1876.